The X-ray spectra of accreting Kerr black holes

Andrew C. Fabian and Giovanni Miniutti

Institute of Astronomy, Madingley Road Cambridge CB3 0HA, UK

February 5, 2008

Abstract

The relativistic broad iron lines seen in the X-ray spectra of several active galaxies and Galactic black hole systems are reviewed. Most such objects require emission from within the innermost stable orbit of a non-rotating black hole, suggesting that the black holes are rapidly spinning Kerr holes. We discuss the soft excess, the broad iron line and the Compton hump characteristic of reflection from partially ionized gas and show that they may be a common ingredient in the X-ray spectra of many radiatively-efficient, accreting black holes. Strong gravitational bending of the radiation close to a Kerr black hole can explain the otherwise puzzling spectral variability seen in some objects. The Narrow Line Seyfert 1 galaxies may be among the most extreme objects yet seen.

arXiv:astro-ph/0507409v1 18 Jul 2005

1   Introduction

The form of the spacetime geometry around an astrophysical black hole (BH) is due to Roy Kerr (1963) who found the exact solution to the general relativistic Einstein's equations for the spacetime outside the horizon of a rotating BH. Since then, rotating BH are known as Kerr BH, the spacetime geometry of which depends on two parameters only, the BH mass and spin. In the limit of no rotation, Kerr's solution coincides with that for a non–rotating BH found earlier by Karl Schwarzschild (1916), which obviously depends on the BH mass only. The complete solution of the equations of motion in the Kerr spacetime is due to Brandon Carter (1968). The interested reader finds an excellent treatment of Einstein's theory of General Relativity and of BH spacetimes in the fundamental book *Gravitation* by Misner, Thorne & Wheeler (1973).

A large fraction of the accretion energy in luminous BH systems is dissipated in the innermost regions of the accretion flow. Most of the power is radiated from close to the smallest accretion disc radii in the relativistic region close to the BH (Shakura & Sunyaev 1973; Pringle 1981). Relativistic effects then affect the appearance of the X–ray spectrum from the disc through Doppler, aberration, gravitational redshift and light bending effects (Page & Thorne 1974; Cunningham 1975, 1976). The dominant feature in the 2–10 keV X–ray spectrum seen by a distant observer is an iron line with a broad skewed profile which carries unique information on the structure, geometry, and dynamics of the accretion flow in the immediate vicinity of the central BH, providing a tool to investigate the nature of the spacetime there (Fabian et al. 1989; Laor 1991).

Relativistic broad iron lines seen in the spectrum of several active galaxies and Galactic black hole binaries are reviewed here (see also Fabian et al 2000; Reynolds & Nowak 2003 for previous reviews). Among others, the cases for relativistic lines in the Seyfert galaxies MCG–6-30-15 and IRAS 18325–5926, and the X-ray binaries XTE J1650–500 and GX 339-4 are very strong (Tanaka et al 1995; Wilms et al 2001; Fabian et al 2002a; Iwasawa et al 1996a; Iwasawa et al 2004; Miller et al 2002a; Miniutti, Fabian & Miller 2004; Miller et al 2004a,b). In three out of four objects, the X–ray data require emission from within the innermost stable circular orbit of a non–rotating BH, suggesting that the BHs in many objects are rapidly spinning. The spectra of many other objects, in particular Narrow Line Seyfert 1 (NLS1) galaxies, can be successfully described by a simple two–component model comprising a highly variable power law continuum and a much more constant reflection component from the accretion disc (e.g. Fabian et al 2004; Fabian et al 2005; Ponti et al 2005). The puzzling spectral variability of such sources is now beginning to be understood within the context of emission from the strong gravity regime (Miniutti et al 2003; Miniutti & Fabian 2004). Some active galactic nuclei (AGN) and X-ray black hole binaries show either no line or only a narrow one (e.g. Page et al 2004; Yaqoob & Padmanabhan 2004). This is discussed within the context of both theoretical implications and present observational limitations. Finally, the short–timescale variability of the broad iron line is beginning to be unveiled, providing exciting results that are dramatically improving our understanding of the innermost regions of the accretion flow, where General Relativity is no longer a small correction and becomes the most relevant physical ingredient (e.g. Turner et al 2002; Iwasawa, Miniutti & Fabian 2004).

The advent of future X–ray missions with higher energy resolution (e.g. *Suzaku* succesfully launched in July 2005) and much larger collecting area in the relevant iron band (XEUS and Constellation–X in the next decade) will open up a new window on the innermost regions of the accretion flow in AGN and X–ray binaries. This will enable us to further test the general picture we propose here, with the potential of mapping with great accuracy the strong field regime of General Relativity in a manner which is still inaccessible at other wavelengths.
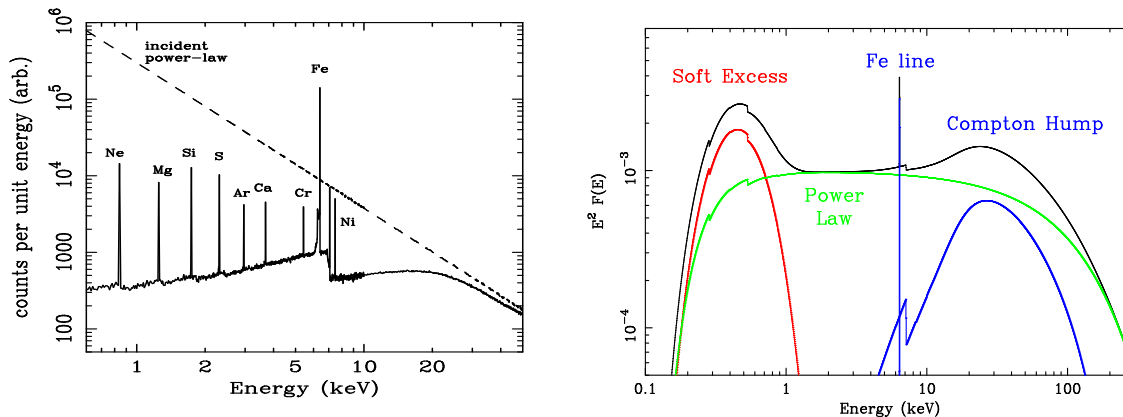
Figure 1: *Left panel*: Monte Carlo simulations of the reflection spectrum from a slab of uniform density neutral matter with solar abundances. The incident power law continuum is also shown. Figure from Reynolds (1996). *Right panel*: The main components of the X–ray spectra of unobscured accreting BH are shown: soft quasi–thermal X–ray emission from the accretion disc (red); power law from Comptonization of the soft X–rays in a corona above the disc (green); reflection continuum and narrow Fe line due to reflection of the hard X–ray emission from dense gas (blue).

2   Main components of the X–ray spectrum

Radiatively-efficient accreting BHs are expected to be surrounded by a dense disc radiating quasi-blackbody thermal EUV and soft X-ray emission (see e.g the seminal paper by Shakura & Sunyaev 1973). However, the X–ray spectra of accreting BHs also exhibit a power law component extending to hard X–ray energies up to 200 keV or more. The most promising physical mechanism to produce such hard power law components is Comptonization of the soft X–ray photons in a corona above the disc, possibly fed by magnetic fields from the body of the disc itself (e.g. Haardt & Marschi 1991 and 1993, Zdziarski et al 1994). Irradiation of the dense disc material by the hard X-rays then gives rise to a characteristic "reflection" spectrum which is the result of Compton scattering and photoelectric absorption followed either by Auger de-excitation or by fluorescent line emission (see e.g. Guilbert & Rees 1988; Lightman & white 1988; George & Fabian 1991, Matt, Perola & Piro 1991). This last process gives rise to an emission line spectrum where fluorescent narrow Kα lines from the most abundant metals are seen. Thanks to a combination of large cosmic abundance and high fluorescent yield, the iron (Fe) Kα line at 6.4 keV is the most prominent fluorescent line in the X–ray reflection spectrum. Photoelectric absorption is an energy–dependent process, so that incident soft X–rays are mostly absorbed, whereas hard photons tend to be Compton scattered back out of the disc. However, above a few tens of keV, Compton recoil reduces the backscattered photon flux and produces a broad hump–like structure around 20–30 keV (the so–called Compton hump). An example of the X–ray reflection spectrum from a neutral and uniform density semi–infinite slab of gas is shown in the left panel of Fig. 1 where fluorescent emission lines dominate below about 8 keV and the Compton hump is seen above 20 keV (from Reynolds 1996).

In the case of AGNs, the accretion disc is not the only reflector able to produce a X–ray reflection spectrum. The presence of a dusty molecular torus surrounding the accreting system is required by unification models at the parsec scale (Antonucci 1993). The torus provides the absorbing column (sometimes more than 10^{24} cm^{-2}) that is observed in Seyfert 2 galaxies which are thought to be distinguished from unobscured Seyfert 1 galaxies only because of a higher observer inclination. The torus itself is Compton–thick and therefore provides an additional reflector producing a spectrum very similar to that seen in the
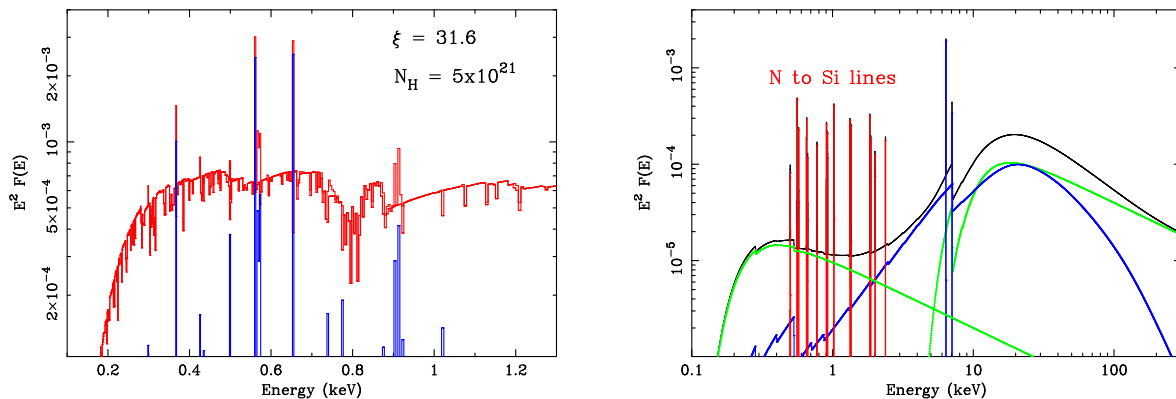
Figure 2: *Left panel*: The effect of photoionized gas surrounding an AGN is shown both in absorption (red) and emission (blue). The spectrum is from the XSTAR code of Kallman & Krolik (1986). *Right panel*: The typical spectrum of a Seyfert 2 galaxy. The primary continuum (green) is heavily absorbed by a large column (typically larger than 10^{24} cm^{-2}) which is identified as the torus, partially blocking the line of sight. The same column produces nearly neutral X–ray reflection (blue) from the visible side of the torus. Emission lines due to photoionized gas (red) are detectable because of the reduced primary continuum flux.

left panel of Fig. 1. As will be explained in detail in the next section, special and general relativistic effects shape the reflection spectrum from the centre of the accretion disc and not that from regions far away from the central BH (such as the torus), helping us to disentangle the two contributions.

In the right panel of Fig 1, we show the main components of the X–ray spectrum of accreting black holes. The "soft excess" represents here the soft X–ray emission from the disc, although some other interpretations are possible and will be discussed throughout this contribution. We also show the power law (with a high energy cut–off characteristic of the coronal temperature) and reflection components. Reflection is here represented by the reflection continuum (characterised by the "Compton hump") and the Fe Kα line at 6.4 keV that we assume here to be narrow, i.e. emitted from a distant reflector such as the torus. The spectrum is absorbed by a column of 2×10^{20} cm^{-2}, representing the typical value for absorption by our Galaxy in the line of sight.

Another important component in the X–ray spectrum of AGN is due to the ubiquitous presence of warm gas surrounding the central nucleus. This gas is photoionized by the primary X–ray continuum and contributes to the spectrum both in absorption and in re–emission (Halpern 1984; Reynolds 1997; Kaastra et al 2000; Kaspi et al 2001). In the case of Seyfert 1 galaxies, the continuum level is so high that the emission component is diluted and generally not observable, except in particularly low flux states of the X–ray source. One remarkable case in this sense is provided by the low flux state of NGC 4051 (see the analysis of the high resolution *XMM-Newton*–RGS data below 2 keV by Pounds et al 2004b; also Ponti et al 2005).

In Seyfert 2 galaxies, the primary continuum is heavily absorbed by large columns in the line of sight (the torus) and therefore the emission component is readily detectable. On the other hand, absorption by this same photoionized gas is obviously easier to detect in Seyfert 1 than Seyfert 2 galaxies due to the higher level of the continuum. In the left panel of Fig. 2 we show both absorption and emission components on a primary power law continuum (plus cold absorption from our own Galaxy in the direction of the source) in the most relevant soft X–ray band. The gas is assumed to have a column of $N_{\mathrm{H}} = 5 \times 10^{21}$ cm^{-2} and ionization parameter of $\xi = 31.6$ erg cm s^{-1} and the spectrum is modelled with the XSTAR code (Kallman & Krolik 1986). In the right panel of the same figure, we show a qualitative view of the typical spectrum for a Seyfert 2 galaxy. The hard spectrum is dominated by reflection from
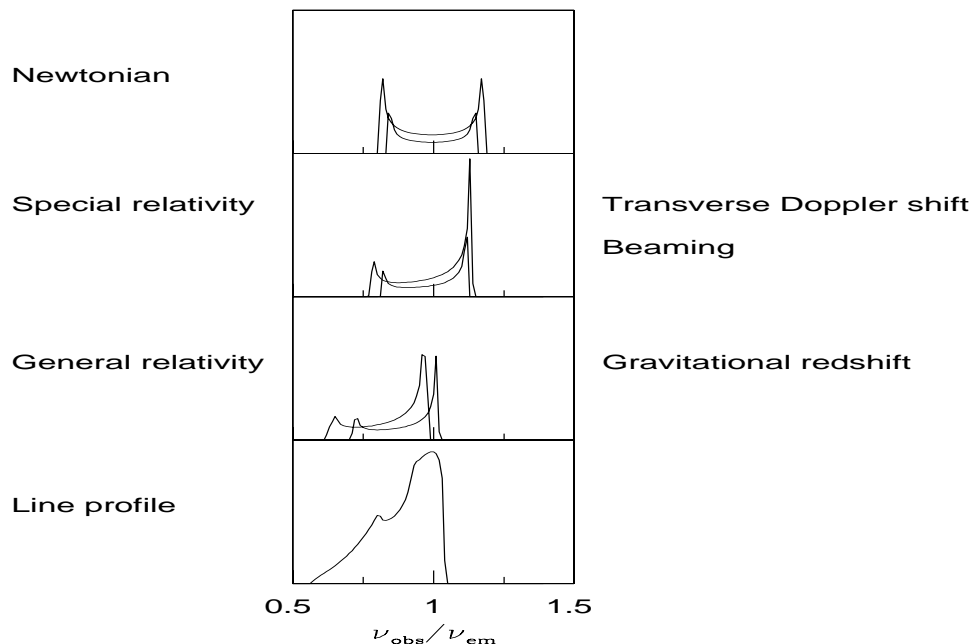
Figure 3: The profile of an intrinsically narrow emission line is modified by the interplay of Doppler/gravitational energy shifts, relativistic beaming, and gravitational light bending occurring in the accretion disc (from Fabian et al 2000). The upper panel shows the symmetric double–peaked profile from two annuli on a non–relativistic Newtonian disc. In the second panel, the effects of transverse Doppler shifts (making the profiles redder) and of relativistic beaming (enhancing the blue peak with respect to the red) are included. In the third panel, gravitational redshift is turned on, shifting the overall profile to the red side and reducing the blue peak strength. The disc inclination fixes the maximum energy at which the line can still be seen, mainly because of the angular dependence of relativistic beaming and of gravitational light bending effects. All these effects combined give rise to a broad, skewed line profile which is shown in the last panel, after integrating over the contributions from all the different annuli on the accretion disc.

the torus, whereas in the soft band emission lines from photoionized gas can be detected because of the low continuum level (e.g. Kinkhabwala et al 2002; Bianchi et al 2005 and many others). In the following we shall focus on unobscured accretion systems such as Sefert 1 galaxies and BH binaries in which the innermost regions of the accretion flow are in principle observable.

3   The relativistic iron line

The Fe I Kα emission line is a doublet comprising Kα1 and Kα2 lines at 6.404 keV and 6.391 keV respectively. However, the energy separation has generally been too small to be detected and a weighted mean at 6.4 keV is generally assumed. The resulting line is symmetric and intrinsically much narrower than the spectral resolution commonly available today[1]. Hence, the detailed line shape and broadening can be used to study the dynamics of the emitting region.

If the reflection spectrum, and therefore the Fe line, originates from the accretion disc, the line shape is distorted by Newtonian, special and general relativistic effects (see e.g. Fabian et al 2000). This is illustrated schematically in Fig. 3. In the Newtonian case, each radius on the disc produces a symmetric

---

[1]*Suzaku* will soon provide the high energy resolution needed to resolve the Kα1 and Kα2 lines
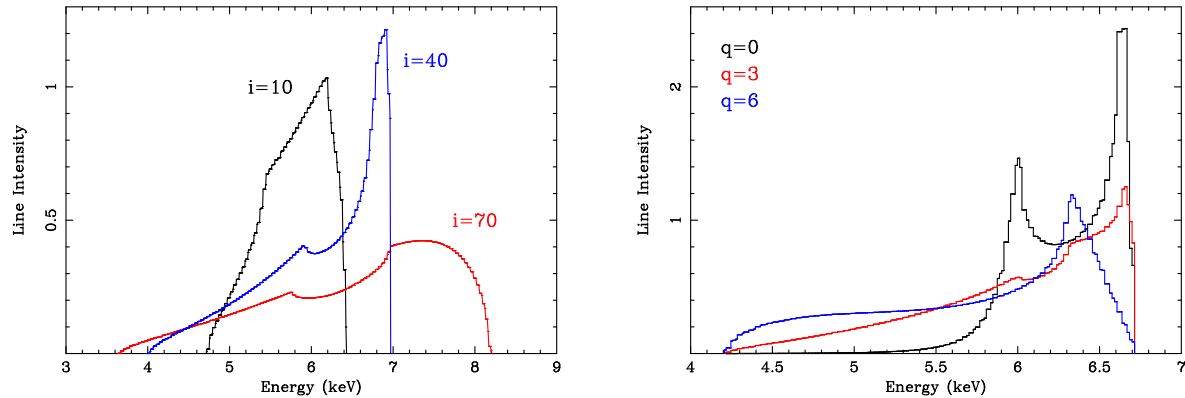
Figure 4: *Left panel*: The dependence of the line profile on the observer inclination is shown. *Right panel*: The dependence of the line profile on the emissivity profile on the disc is shown. The disc emissivity is assumed to scale as $\epsilon = r^{-q}$. The steeper the emissivity, the broader and more redshifted the line profile, because more emphasis is given to the innermost radii where gravity dominates.

double–peaked line profile with the peaks corresponding to emission from the approaching (blue) and receding (red) sides of the disc. Close to the BH, where orbital velocities become relativistic, relativistic beaming enhances the blue peak with respect to the red one, and the transverse Doppler effect shifts the profile to lower energies. As we approach the central BH and gravity becomes strong enough, gravitational redshift becomes important with the effect that the overall line profile is shifted to lower energies. The disc inclination fixes the maximum energy at which the line can still be seen, mainly because of the angular dependence of relativistic beaming and of gravitational light bending effects. Integrating over all radii on the accretion disc, a broad and skewed line profile is produced, such as that shown in the bottom panel of Fig. 3. It is clear from the above discussion that the detailed profile of a broad relativistic line from the accretion disc has the extraordinary potential of revealing the dynamics of the innermost accretion flow in accreting BHs and even of testing Einstein's theory of General Relativity in a manner that is unaccessible to other wavelengths.

3.1   Dependence on disc inclination and emissivity

The relativistic line profile exhibits a dependence for many physical parameters. The energy of the blue peak of the line is mainly dictated by the inclination of the observer line of sight with respect to the accretion disc axis. This is clear in the left panel of Fig. 4 where we show the result of fully relativistic computations (e.g. Fabian et al 1989; Laor 1991; Dovčiak, Karas & Yaqoob 2004 among many others). The three profiles have all the same parameters but different observer inclination i. From the Figure, it is clear that the higher the inclination the bluer the line is, providing a quite robust tool to measure the inclination of the accretion disc.

Another important parameter is the form of the emissivity profile, i.e. the efficiency with which the line is emitted as a function of the radial position on the disc. This depends mainly on the illumination profile by the hard X–rays from the corona which is in turn determined by the energy dissipation on the disc and by the heating events in the corona (possibly associated with magnetic fields see e.g. Merloni & Fabian 2001a,b). The emissivity profile is generally assumed to be in the form of a simple power law $\epsilon(r) = r^{-q}$, where q is the emissivity index (but see e.g. Beckwith & Done 2004). By assuming that the emissivity is a good tracer of the energy dissipation on the disc, the standard value for the emissivity index is $q = 3$ (e.g. Pringle 1981; also Reynolds & Nowak 2003 and Merloni & Fabian 2003 for a

discussion on the dependence of the emissivity profile on boundary conditions). In the right panel of Fig. 4, we show the dependence of the line profile from this most important parameter. We show the cases of a uniform ($q = 0$), standard ($q = 3$), and steep ($q = 6$) emissivity profile. A steep emissivity profile indicates that the conversion of the X–ray photons from soft to hard in the corona is centrally concentrated thereby illuminating more efficiently the very inner regions of the accretion disc. As shown in the figure, steeper emissivity profiles produce much broader and redshifted lines because more weight is given to the innermost disc, where gravitational redshift dominates.

3.2 Self–consistent ionized reflection models

So far, we have assumed that the disc (or to be more precise its outer layers) is a slab of uniform density gas where hydrogen and helium are fully ionized, but all the metals are neutral. The real situation is likely to be much more complex. One first important step towards the accurate model of accretion disc atmospheres is made by considering thermal and ionization equilibrium. Results of such computations have been published over the last ten years or so with different degrees of complexity (e.g. Ross & Fabian 1993; Matt, Fabian & Ross 1993, 1996; Zycki et al 1994; Nayakshin, Kazanas & Kallman 2000; Rózańska et al 2002; Dumont et al 2003). See Ballantyne, Ross & Fabian 2001 for a comparison between different hypothesis such as constant–density atmospheres and atmospheres in hydrostatic equilibrium. The recent work by Ross & Fabian (2005) extending and improving previous computations (e.g. Ross, Fabian & Young 1999; Ballantyne, Ross & Fabian 2001) is described here in some detail since it is used extensively in comparing X–ray data to theoretical models.

The illuminating radiation is assumed to have an exponential cut–off power law form with high–energy cut–off fixed at 300 keV and variable photon index Γ between 1 and 3 roughly covering the observed range. The ionization parameter ξ is defined as the ratio between the isotropic total illuminating flux and the comoving hydrogen number density of the gas; results are produced for ξ ranging from 1 erg cm s^{-1} to 10^4 erg cm s^{-1}. The local temperature and fractional ionization of the gas are computed self–consistently by solving the equations of thermal and ionization equilibrium and ions from C, N, O, Ne, Mg, Si, S, and Fe are treated. The available model grids allow for a variable Fe abundance.

In the left panel of Fig. 5 we show X–ray reflection spectra produced by the code for three different values of the ionization parameter (all other parameters being fixed). The ionization parameter has clearly a large effect on the resulting spectrum, most remarkably on the emission lines. For $\xi = 10^4$ erg cm s^{-1} (top black) the surface layer is very highly ionized and the only noticeable line is a highly Compton–broadened Fe Kα line peaking at 7 keV. The overall spectral shape closely resembles that of the illuminating continuum (a cut–off power law with photon index $\Gamma = 2$). For $\xi = 10^3$ erg cm s^{-1} (middle blue) the strong Fe Kα line is dominated by the Fe XXV intercombination line, while Kα lines from the lighter elements emerge in the 0.3-3 keV band. Further reducing the ionization parameter to $\xi = 10^2$ erg cm s^{-1} gives rise to a spectrum dominated by emission features below 3 keV atop a deep absorption trough. The most prominent feature is the Fe Kα one at 6.4 keV. No residual Compton broadening of the emission lines is visible.

In the right panel of Fig. 5 we show two versions of a model with an ionization parameter of $\xi = 2 \times 10^2$ erg cm s^{-1}. The blue one is the X–ray reflection spectrum in the absence of any relativistic effect, whereas in red we show the relativistically–blurred version of the same model, i.e. the spectrum that is observed if reflection occurs from the accretion disc. All sharp spectral features of the unblurred spectrum (blue) are broadened by the relativistic effects explained above which makes it difficult to identify clear emission lines in the soft spectrum. Below about 2 keV the situation is often complicated by the presence of absorption/emission features due to photoionized gas complicating the soft part of the spectrum (see Fig. 2, left panel). Thanks to its strength, isolation, and to the fact that it occupies a region of the X–ray
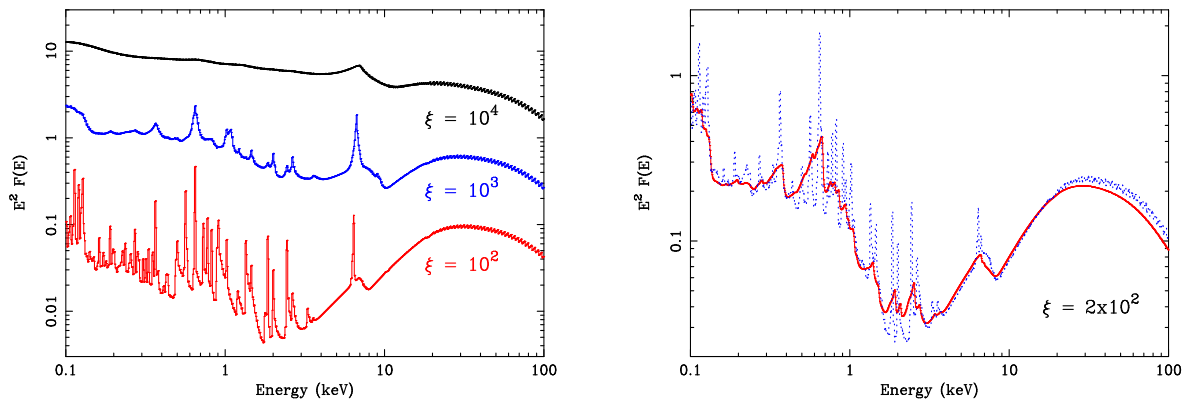
Figure 5: *Left panel*: Computed X–ray reflection spectra as a function of the ionization parameter ξ (from the code by Ross & Fabian 2005). The illuminating continuum has a photon index of $\Gamma = 2$ and the reflector is assumed to have cosmic (solar) abundances. *Right panel*: Relativistic effects on the X–ray reflection spectrum. We assume that the intrinsic rest–frame spectrum (dotted blue) is emitted in an accretion disc and suffers all the relativistic effects discussed above (see text for details). The relativistically–blurred reflection spectrum is shown in red.

spectrum relatively free from absorption, the Fe line is however clearly seen. This is what makes this particular emission feature a remarkable and unique tool that allows us to investigate the dynamics of the innermost accretion flow via relativistic effects in accreting BH systems.

3.3   Dependence on the inner disc radius

Einstein's equations imply the existence of an innermost radius within which the circular orbit of a test particle in the equatorial plane is no longer stable. This radius is known as the Innermost Stable Circular Orbit (ISCO), sometimes referred to as the marginally stable orbit (Bardeen, Press & Teukolsky 1972). Beyond the ISCO, test particles rapidly plunge into the BH on nearly geodesic orbits with constant energy and angular momentum. By making the standard assumption that the accretion disc is made of gas particles in circular, or nearly circular, orbital motion, the disc extends down to the ISCO, and emission from the plunging region is ignored. We shall discuss further this assumption in the next Section.

The actual radius of the ISCO depends on the BH spin parameter a/M which can take any value for 0 (Schwarzschild BH) to 1 (maximally spinning Kerr BH). As pointed out by Thorne (1974), the maximal value for the spin parameter is likely to be about 0.998 and we shall refer to that case as "Maximal Kerr". The dependence of the ISCO from the BH spin parameter is illustrated in the left panel of Fig. 6. The ISCO lies at $6\ r_g$ from the centre for a Schwarzschild BH, and at $\simeq 1.24\ r_g$ for a Maximal Kerr one, where $r_g = GM/c^2$ is the gravitational radius. It should be stressed that the dependence is quite steep. If emission from say $3\ r_g$ can be detected the implied BH spin would be $a/M > 0.78$. Notice that accretion naturally causes a BH to spin up provided the disc angular momentum is oriented as that of the hole (the possible history of the spin of massive BHs is discussed e.g. by Volonteri et al 2005 and references therein).

The inner boundary of the accretion disc, i.e. the location of the ISCO, has a large impact on the shape of the line profile, especially on its broad red wing. This is shown in the right panel of Fig. 6 where the cases of a Schwarzschild (red) and Maximal Kerr BH (blue) are computed. The line is much broader in the Kerr case because the smaller inner disc radius implies that the line photons are suffering stronger relativistic effects (such as gravitational redshift) which is visible in the resulting line profile. To summarise, the detection and modelling of a relativistic broad Fe line via X–ray observations of accreting BH potentially provides crucial information on the system inclination, the radial efficiency of the coronal
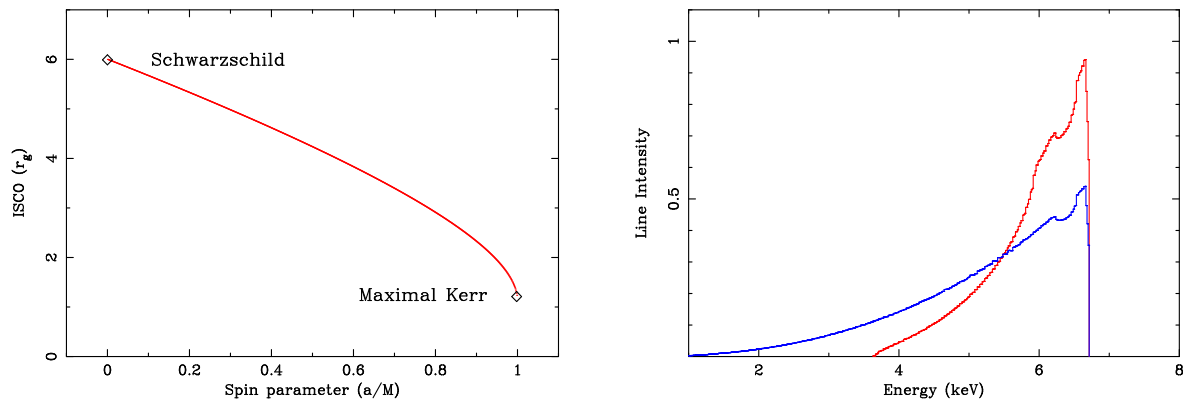
Figure 6: *Left panel*: The dependence of the ISCO from the BH spin. We consider the allowed spin range from $a/M = 0$ (Schwarzschild solution) to $a/M = 0.998$ (Maximal Kerr solution). For these extremal cases, the ISCO is located at 6 r_g ($a/M = 0$) and $\simeq 1.24\ r_g$ ($a/M = 0.998$). *Right panel*: The line profiles dependence from the inner disc radius is shown for the two extremal cases of a Schwarzschild BH (red, with inner disc radius at 6 r_g) and of a Maximal Kerr BH (blue, with inner disc radius at $\simeq 1.24\ r_g$)

hard X–ray emission, and also on one of the two parameters that characterise the Kerr solution, i.e. the BH spin.

3.4   The ISCO and its relation to black hole spin

A key issue in using the profile of a broad iron line to determine BH spin is whether the derived inner radius equals the ISCO, or not. Reynolds & Begelman (1997) pointed out that matter in the plunge region within the ISCO can also contribute to reflection and so could confuse spin determination. The matter in the plunge region is however moving inward rapidly and so has a low density. This means that the ionization parameter is high, which changes the ability to produce a detectable iron line. Young, Ross & Fabian (1998) showed in the key case of MCG–6-30-15 that the emission (and absorption) produced by reflection in the plunge region does not resemble the observed line shape. The issue of matter falling within the ISCO was further considered by Gammie (1999) and Krolik (1999); see also Agol & Krolik (2000) with the inclusion of magnetic fields which can connect the outer part of the plunge region with the disc and slow matter down (also Krolik & Hawley 2002). In fact, Dovčiak, Karas & Yaqoob (2004) have shown that the difference in the flow direction has a negligible effect on the profile shape.

We suspect that the effect of magnetic fields on the iron-line appearance is small. The ionization parameter can be written as

$$\xi = 3 \times 10^7 f(v_{\rm rad}/c) \quad \text{erg cm s}^{-1}\ , \tag{1}$$

where f is the volume filling factor of the flow which is falling radially inward at velocity $v_{\rm rad}$ (Fabian & Miniutti, in preparation). Since f and $v_{\rm rad}$ are unlikely to be much smaller than 0.1 over most of the plunge region, it is most unlikely that a strong iron line, requiring $\xi \sim 100$–1000 erg cm s^{-1}, can be produced. We suspect that the inner radius determined from iron line studies cannot originate from far within the ISCO and that the inner disc radius $r_{\rm in}$ is never more than one $r_{\rm g}$ or so within the ISCO.
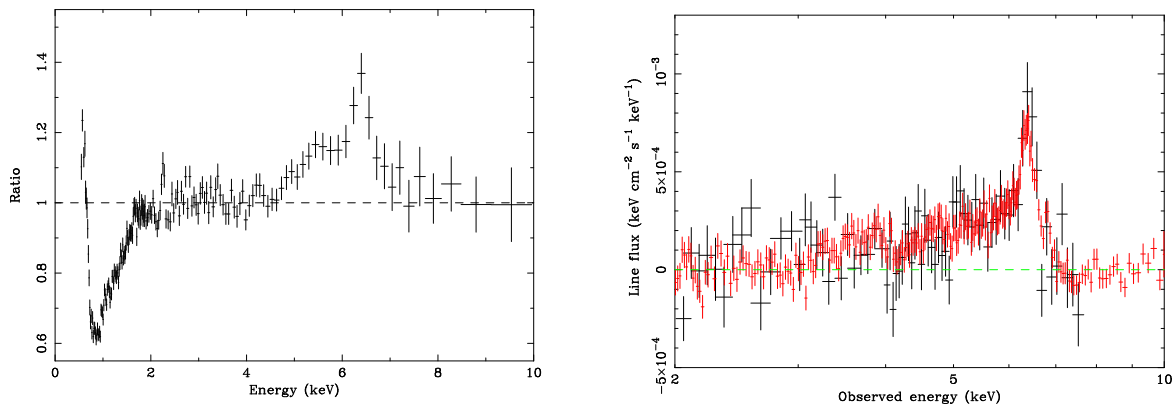
Figure 7: *Left panel*: Ratio to a power law model of the 1994 ASCA S0 spectrum of MCG–6-30-15. The broad Fe line is clearly detected, together with absorption from photoionized gas below 2 keV. *Right panel*: Superposition of the broad Fe line profile of MCG–6-30-15 from the long *XMM-Newton* (red) and *Chandra* (black) observations. The observations are non–simultaneous but the line profiles superimpose very well (Young et al 2005).

4   The broad relativistic Fe line of MCG–6-30-15

The X-ray spectrum of the bright Seyfert 1 galaxy MCG–6-30-15 ($z = 0.00775$) has a broad emission feature stretching from below 4 keV to about 7 keV. The shape of this feature, first clearly resolved with *ASCA* by Tanaka et al. (1995), is skewed and peaks at about 6.4 keV. This profile is consistent with that predicted from iron fluorescence from an accretion disc inclined at 30 deg extending down to within about 6 gravitational radii ($6r_{\mathrm{g}} = 6GM/c^2$) of a BH. During the *ASCA* observation the line appeared to be occasionally redshifted to lower energies, implying emission from even smaller radii and therefore strongly suggesting that the BH in this object is rapidly spinning (Iwasawa et al 1996b). The broad iron line of MCG–6-30-15 has been detected by all major X–ray mission (*ASCA*, *RXTE*, *BeppoSAX*, *Chandra*, and *XMM-Newton*) with very similar results.

In Fig. 7 we show the line profile obtained at different times with three different detectors. In the right panel, we show the broadband spectrum (as a ratio with a power law model) of the S0 detector on board of *ASCA* during the 170 ks observation in 1994 (Iwasawa et al 1996b). In the right panel, we show the line profile from non–simultaneous *XMM-Newton* (red, 320 ks in 2001) and *Chandra* (black, 522 ks in 2004) observatories (Fabian et al 2002a; Young et al 2005). The large effective area provided by *XMM-Newton* confirmed earlier results by Iwasawa et al (1996b; 1999) showing that the broad red wing of the line extends down to about 3 keV implying a spin parameter $a/M > 0.93$ (Dabrowski et al. 1997; Reynolds et al. 2004). Here we report in some detail results from the *XMM-Newton* observations of MCG–6-30-15 (Wilms et al 2001; Fabian et al 2002a; Fabian & Vaughan 2002; Vaughan & Fabian 2004; Reynolds et al 2004) mentioning also the most important consequences of the recent long *Chandra* observation (Young et al 2005).

The 2001 *XMM-Newton* observation was very long (about 320 ks corresponding to three full satellite orbits) and simultaneous with a *BeppoSAX* one, providing unprecedented spectral coverage with *XMM-Newton* being more sensitive than *BeppoSAX* in the 0.2–10 keV band, and *BeppoSAX* extending the data set up to 200 keV. The broadband *XMM-Newton* light curve for the three orbits is shown in the left panel of Fig. 8. In the right panel of the same figure we show the observed broad Fe line profile from the time–averaged spectrum. We discuss here our best description of the X–ray spectrum of MCG–6-30-15, focusing on the broad Fe line, and later review alternatives to our modelling which, however, all prove
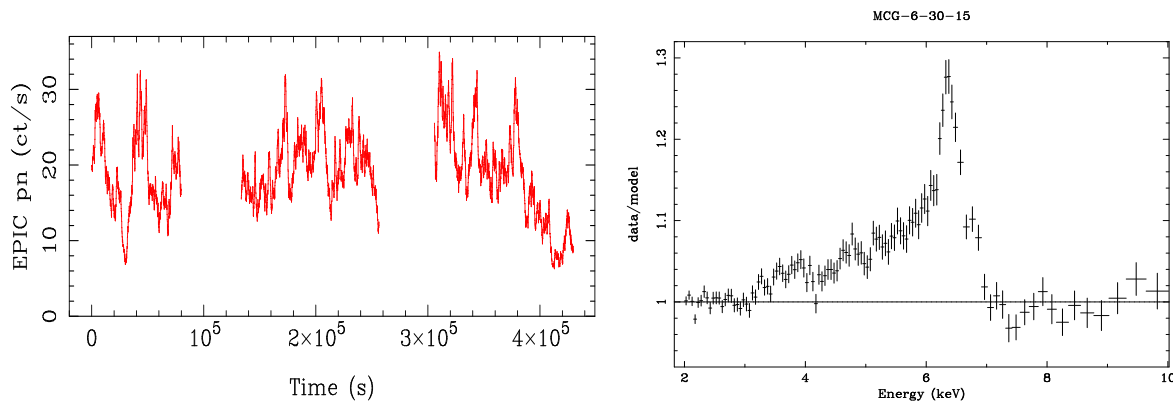
Figure 8: *Left panel*: The broadband light curve of the long *XMM-Newton* observation in 2001. Three satellite's orbits have been devoted to study MCG–6-30-15 in 2001, for a total exposure of about 320 ks. *Right panel*: The broad iron line in MCG–6-30-15 from the *XMM-Newton* observation in 2001 (Fabian et al. 2002a) is shown as a ratio to the continuum model.

largely unsatisfactory when tested against the data.

The broadband spectrum of MCG–6-30-15 is best described by a relativistically blurred reflection spectrum modified by absorption by photoionized gas below about 2 keV (Fabian et al 2002a). For the X–ray reflection model, we used the code by Ross & Fabian (1993; 2005) allowing the photon index Γ, the ionization parameter ξ, and the relative strength of the reflection spectrum with respect to the power law continuum free to vary. To account for Doppler and gravitational effects, the reflection spectrum is convolved with a relativistic kernel computed using a modified version of the code by Ari Laor (1991) which is appropriate for the Maximal Kerr case. However, the inner disc radius is not fixed to the ISCO but can be larger. Therefore, if the inner disc radius can be inferred from the data, information on the spin can in principle be obtained by making use of the ISCO–spin relation (see Fig. 6). The emissivity profile has the general form of a broken power law with index q_{in} from the inner disc radius to a break radius r_{br} and q_{out} outwards.

The best–fitting parameters indicate a weakly ionized disc with ionization parameter $\xi < 30 \, \mathrm{erg\,cm\,s^{-1}}$ and a strong reflection fraction[2] of about $R \simeq 2.2$, a result which is fully confirmed by the *BeppoSAX* data where the Compton hump around 20–30 keV is clearly seen. Fe is measured to be three times more abundant than standard (solar). The parameters of the relativistic blurring are the disc inclination $i = 33° \pm 1°$, the inner disc radius $r_{in} = 1.8 \pm 0.1 \, r_g$, and the emissivity parameters $q_{in} = 6.9 \pm 0.6$, $q_{out} = 3.0 \pm 0.1$, and $r_{br} = 3.4 \pm 0.2$ (Vaughan & Fabian 2004). The measured value of the inner disc radius implies emission from far beyond the ISCO of a Schwarzschild BH ($6 \, r_g$) and therefore suggest the BH in MCG–6-30-15 is rapidly spinning. If we take the measured value of r_{in} as a measure of the ISCO, we can constrain the BH spin to be $a/M = 0.96 \pm 0.01$, providing one of the most remarkable indications so far for the astrophysical relevance of the Kerr solution to the Einstein's equations. The inferred emissivity profile indicates a standard emissivity from about $3.4 \, r_g$ to the outer disc boundary. However, a steep profile is required in the innermost few gravitational radii, indicating that most of the accretion power is released in the region where General Relativity is in the strong field regime. Tapping of black holes spin by magnetic fields in the disc is a strong possibility to account for the peaking of the power so close to the hole (Wilms et al. 2001; Reynolds et al. 2004; Garofalo & Reynolds 2005).

---

[2]The reflection fraction (R) is defined as the relative normalization of the reflection component with respect to the illuminating continuum. $R = 1$ means that the primary source subtends a solid angle $\Omega/2\pi = 1$ at the disc. Values larger than 1 imply that the disc is seeing more illuminating continuum that any observer at infinity and therefore that the primary source is anisotropic and preferentially shines towards the disc.

4.1   Alternatives to a relativistic line

The claim that iron line studies are probing the strong field regime of General Relativity just few gravitational radii from the BH is a bold one, and should always be tested again alternative models. In this spirit, we discuss here alternatives to the broad relativistic Fe line in the X–ray spectrum of MCG–6-30-15 (see also Fabian et al 1995; Fabian et al 2000).

The broad Fe line profile seen in the right panel of Fig. 8 comprises two main components: a relatively narrow core peaking around 6.4 keV, and an extended broad red wing from about 3 keV to 6 keV. If the broad red wing is not due to a relativistic line but instead to some spectral curvature independent of any relativistic effect, we are left with the line core only. If this is emitted from far the BH (such as from the torus), it has to be narrow and unresolved at the *XMM-Newton* resolution (about 100 eV). However, the line core itself is unambiguously resolved by *XMM-Newton*. When modelled by a Gaussian emission line, the line core width is $\sigma = 352^{+106}_{-50}$ eV, much larger than the spectral resolution (Vaughan & Fabian 2004). Considering a blend of lines from different Fe ionization states as responsible for the broadening produces an unacceptable fit. Therefore, even ignoring for a moment the broad red wing of the line, the relatively narrow line core itself already suggest that the line is emitted in a fast orbiting medium close to the central BH and excludes any strong contribution from a reflector located at the parsec (and even sub–parsec) scale such as the torus and/or the Broad Line Region. A small contribution is possible and likely, but at the level of 15 per cent maximum of the line core.

As for the broad red wing of the line below 6 keV (see right panel of Fig. 8) several attempts have been made to explain the spectral shape without invoking relativistic effects. The broad red wing of the line has been modelled by different emission components, i.e. a thermal component, a blend of broadened emission lines (other than Fe), and complex absorption. In the latter model, which is probably the only serious one, the continuum passes through a large column of moderately ionized gas which can cause significant curvature above the Fe L edge (about 0.7 keV) up to about 5–6 keV, therefore with the potential of reproducing the broad red wing of the line. The gas must be sufficiently highly ionized to avoid undetected excessive opacity in the soft band, but not so highly ionized to lose of all its L–shell electrons. The best–fit ionized absorption model to both *XMM-Newton* and *Chandra* data can reproduce the red wing of the line (though the fit statistic is much worse than when the data are fitted with a relativistic line). However, the model predicts a clear complex of narrow absorption lines between 6.4 keV and 6.7 keV. This is inconsistent with the high resolution *Chandra* data as shown in the left panel of Fig. 9 from Young et al (2005). We conclude that ionized absorption cannot reproduce the broad red wing of the relativistic Fe line.

A neutral partial covering model (which would be consistent with *Chandra* data) is also ruled out because it is inconsistent with the high energy data provided by *RXTE* and *BeppoSAX*, in particular the unambiguous requirement for a strong reflection component (Reynolds et al 2004; Vaughan & Fabian 2004). As a further test, a partial covering model was added to the best–fit model with a relativistic line to see if the derived parameters (most importantly the inner disc radius providing information on the BH spin) are robust. No differences were noticed and r_{in} remains at 1.8 ± 0.1 r_g (Vaughan & Fabian 2004; Young et al 2005). An ionized partial covering model can not be simply ruled out, but *Chandra* data constrain the covering fraction to be less than 5 per cent, insufficient to produce enough spectral curvature in the relevant energy band, therefore requiring the presence of a broad relativistic line as for the neutral partial covering model above. As discussed in the next Section, the presence of complex absorption above 3 keV is also strongly (and in our opinion, unambiguously) ruled out by spectral variability analysis.
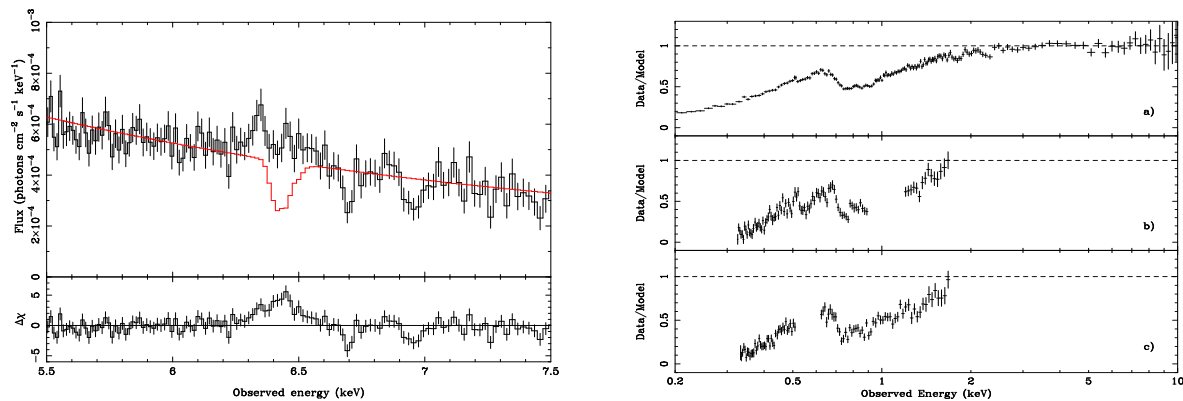
Figure 9: *Left panel*: The *Chandra* HEG spectrum (black) is overlaid to the best–fit ionized absorption model of the broad red wing of the iron line. The ionized absorber produces a curved spectral shape that approximates the broad red wing, but predicts iron absorption features in the 6.4–6.6 keV range (rest–frame) which are inconsistent with the data (Young et al 2005). *Right panel*: The difference spectrum obtained by subtracting the low flux state spectrum from the high flux state one, plotted as a ratio to a power law in the 3–10 keV band. The top panels refers to the EPIC–pn data, the two lower panels to the RGS gratings on *XMM-Newton* (Turner et al 2003).

4.2   A puzzling spectral variability

The X-ray continuum emission of MCG–6-30-15 is highly variable (see Vaughan, Fabian & Nandra 2003; Vaughan & Fabian 2004; Reynolds et al. 2004; McHardy et al 2005 for some recent analyses) as is also clear from the light curve in Fig. 8. Several different methods are used to explore the spectral X–ray variability in accreting BH sources. One such a method is provided by the analysis of the so–called difference spectrum, i.e. the spectrum that can be obtained by subtracting a low flux state spectrum from a high flux one (Fabian & Vaughan 2003). In this way any component that remained constant within the two flux levels is effectively removed from the spectrum which therefore carries information on the variable components plus absorption only. The *XMM-Newton* 2001 observation was split into 2 different flux states according to the light curve (left panel of Fig. 8) and two spectra were extracted as representative of the high and low flux states. The low flux spectrum was then subtracted from the high flux one.

In the right panel of Fig. 9 we show the resulting difference spectrum as a ratio to a power law fitted in the 3–10 keV band (from Turner et al 2003). The EPIC–pn data are shown in the upper panel, while the high resolution *XMM-Newton*–RGS gratings are plotted in the middle and lower panels. It is clear from the figure, that the variable component is very well described by the power law in the 3–10 keV band and is affected by absorption from photoionized gas only below 3 keV. This demonstrates in a model–independent way that the X–ray variability in MCG–6-30-15 is due to a relatively steep ($\Gamma \simeq 2.2$) power law component, and that the amplitude changes of the continuum in MCG–6-30-15 are due to this power law.

The difference spectrum also clarifies in a model–independent way that there is no subtle additional absorption above 3 keV that might influence the broad red wing of the relativistic Fe line. Absorption by either neutral or ionized gas has to show up in the difference spectrum (as seen below 3 keV) but is not detected in the Fe band above 3 keV. This is in our opinion conclusive on the reality of the broad red wing of the Fe line. The case for the relativistic Fe line in MCG–6-30-15 therefore looks even more robust now than before.

It should be stressed that the difference spectrum, unlike the true spectrum of the source, does not exhibit any emission feature (neither narrow nor broad) in the Fe band. This implies that the relativistic Fe line in MCG–6-30-15 is much less variable than the power law continuum and has therefore been removed
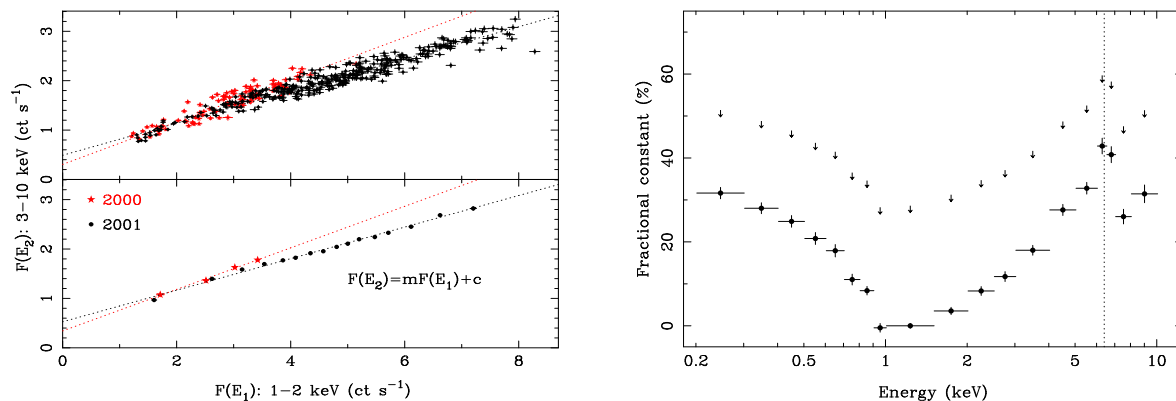
Figure 10: *Left panel*: Flux–flux plot for the 2000 (red) and 2001 (black) *XMM-Newton* observations. The 3–10 keV count rates are plotted versus the simultaneous 1–2 keV count rates. The upper panel shows the raw data, the lower is a binned version of the same plot. *Right panel*: The fractional spectrum of the constant component of MCG–6-30-15 constructed from the y–axis offset in flux–flux plots generated in different bands. The spectrum strongly resembles that of a reflection component, with a prominent contribution at 6.4 keV (vertical dotted line). Figures from Vaughan & Fabian (2004).

by the subtraction. As a test, the *XMM-Newton* 2001 exposure was divided into 10 ks long chunks and spectral fits performed. Direct spectral analysis on the 10 ks spectra confirms that the variability in MCG–6-30-15 closely follows a two–component model comprising a Power Law Component (hereafter PLC) with constant slope of about $\Gamma = 2.2$ and highly variable normalization (a factor 3–4) and a Reflection–Dominated Component (RDC) that carries the broad Fe line and whose variability is confined within 25 per cent (Fabian & Vaughan 2003; Vaughan & Fabian 2004) confirming previous results (Shih, Iwasawa & Fabian 2002; Matsumoto et al 2003).

A further powerful model–independent tool to explore the spectral variability is provided by flux–flux plot analysis which consists of plotting the count rates in two different energy bands against each other (Taylor, Uttley & McHardy 2003). The largest variability in MCG–6-30-15 occurs in the 1–2 keV band which is therefore chosen as the reference energy band. In the left panel of Fig. 10 we show the count rates in the 3–10 keV band plotted against the simultaneous count rates in the 1–2 keV band (from Vaughan & Fabian 2004). Black points refer to the 2001 long *XMM-Newton* observation, red ones to the previous shorter *XMM-Newton* observation in 2000 (Wilms et al 2001). The Figure is divided into two panels, the lower one being simply a binned version. It is clear that a very significant correlation is found in both observations. The scatter in the unbinned version is a manifestation of the different shape of the power spectral density in the two bands and lack of coherence. The scatter is removed in the binned version which is most useful for fitting purposes.

The relationship is clearly linear which is an unambiguous sign that the variability in both bands is dominated by a spectral component which has the same spectral shape and varies in normalization only. However, extrapolating the linear relation to low count rates leaves a clear offset on the y–axis. This strongly suggests the presence of a second component that varies very little and contributes more to the 3–10 keV than to the 1–2 keV band. In other words, the flux in each band is the sum of a variable and a constant component, with the constant component contributing more to the harder than softer energies. From the previous discussion on the difference spectrum, the variable component is easily identified with a power law with constant slope $\Gamma = 2.2$ dominating the variability by variation in normalization only. Moreover, we already know that the reflection component varies little because no Fe line is seen in the difference spectrum and because of the result of direct time–resolved spectral analysis. It is therefore likely that the constant component is associated with the X–ray reflection spectrum, including the relativistic Fe line.
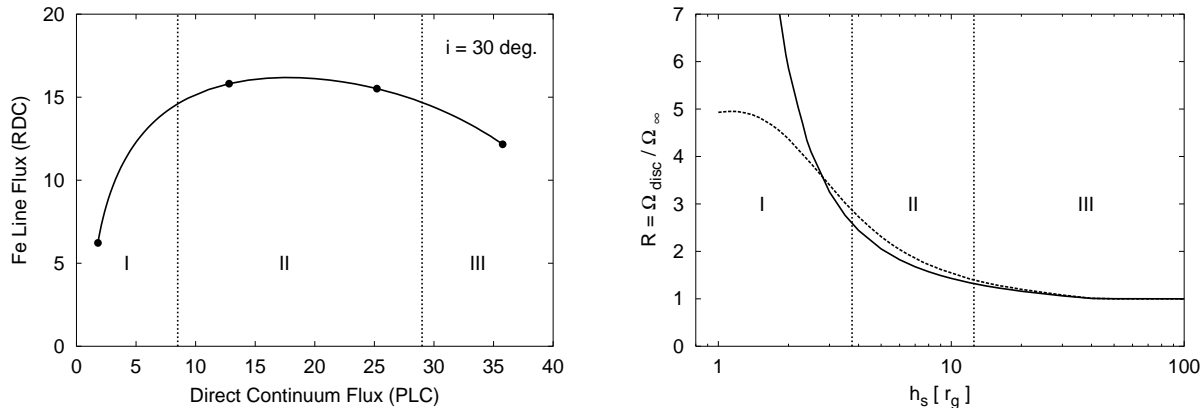
Figure 11: *Left panel*: The Fe line flux (representative of the whole RDC) as a function of the PLC flux observed at infinity. The variability is only due to changes in the primary source height. Black dots represent heights of $h = 1, 5, 10, 20\ r_g$. Three regimes can be identified. In regime II the RDC variation is within 10 per cent while the PLC varies by about a factor 4. *Right panel*: The reflection fraction as a function of the source height (nearly the same if plotted versus the PLC flux). We show the cases of a source on the disc axis (solid) and one at $2\ r_g$ from the axis.

Flux–flux plots can be produced for any chosen band by plotting the relative count rates as a function of those in the reference band. Each plot will produce a different y–axis offset which represents the fractional contribution of the constant component to the spectrum in that particular energy band. Therefore, by recording the value of the offset in each band, the "fractional spectrum" of the constant component can be obtained and the hypothesis that this is similar to a X–ray reflection spectrum can be tested. The fractional spectrum of the constant component is shown in the right panel of Fig. 10 (from Vaughan & Fabian 2004; see Taylor, Uttley & McHardy for an similar result based on *RXTE* data). The black circles are the result obtained by assuming that the contribution of the constant component in the 1–1.5 keV band is null, the arrows indicate the upper limits (notice that the shape, which is the relevant here, does not change). The fractional spectrum is soft below ~ 1 keV and hard at higher energies with a strong contribution at 6.4 keV. This strongly resembles a typical X–ray reflection spectrum, supporting our previous hypothesis that the constant component in MCG–6-30-15 is indeed reflection–dominated.

4.3   Interpretation: the light bending model

If the observed power law component (PLC) continuum drives the iron fluorescence then the line flux should respond to variations in the incident continuum on timescales comparable to the light-crossing, or hydrodynamical time of the inner accretion disc (Fabian et al 1989; Stella 1990; Matt & Perola 1992; Reynolds et al. 1999). This timescale ($\sim 100M_6$ s for reflection from within $10r_g$ around a black hole of mass $10^6 M_6\ \mathrm{M_\odot}$) is short enough that a single, long observation spans many light-crossing times. This has motivated observational efforts to find variations in the line flux (e.g. Iwasawa et al. 1996b, 1999; Reynolds 2000; Vaughan & Edelson 2001; Shih, Iwasawa & Fabian 2002; Matsumoto et al 2003). However, the variability analysis discussed above implies that the reflection–dominated component (RDC) does not follows in general the PLC variations.

Explaining the relatively small variability of the RDC, compared with that of the PLC, provides a significant challenge. The RDC and PLC appear partially disconnected. Since however both show the effects of the warm absorber they must originate in a similar location. As the extensive red wing of the iron line in the RDC indicates emission peaking at only a few gravitational radii (GM/c^2) we must assume that this is indeed where that component originates. On the other hand, this is also the region

where most of the accretion power is dissipated and therefore the PLC must originate in the corona above the innermost disc as well, so that light–travel–time effects cannot be invoked to explain the lack of response of the RDC to the PLC variation.

We have developed a model for the variability of the PLC and RDC components in accreting BH systems which is based on the idea that since both components originate in the immediate vicinity of the BH, they both suffer relativistic effects due to strong gravity (Fabian & Vaughan 2003; Miniutti et al 2003; Miniutti & Fabian 2004). Some of the effects of the strong gravitational field on the line shape and intensity had already been explored by Martocchia, Matt & Karas (2000) and Dabrowski & Lasenby (2001). We assume a geometry in which a Maximal Kerr BH is surrounded by the accretion disc extending down to the ISCO. The PLC is emitted from a primary source above the accretion disc. Its location is defined by its radial distance from the BH axis and its height (h) above the accretion disc. Several geometries have been studied and the results we present are qualitatively maintained for any source location and geometry within the innermost 4–5 gravitational radii from the black hole axis. The main parameter in our model is the height of the primary source above the accretion disc and the main requirement is for the source to be compact. The primary PLC source could be physically realised by flares related to magnetic reconnection in the inner corona, emission from the base of a jet close to the BH, internal shocks in aborted jets, dissipation of the rotational BH energy via magnetic processes, etc. Any mechanism producing a compact PLC–emitting region above the innermost region of the accretion flow would be relevant for our model (e.g. Blandford & Znajek 1977; Markoff, Falcke & Fender 2001; Li 2003; Ghisellini, Haardt & Matt 2004 and many others).

A fraction of the radiation emitted by the primary source directly reaches the observer at infinity and constitutes the direct continuum which is observed as the PLC of the spectrum. The remaining radiation illuminates the accretion disc (or is lost into the hole event horizon). The radiation that illuminates the disc is reprocessed into the RDC. For simplicity, we assume that the intrinsic luminosity of the primary source is constant. The basic idea is that the relevant parameter for the variability of both the PLC and the illuminating continuum on the disc (which drives the RDC variability) is the height of the primary source above the accretion disc and that the variability is driven by general relativistic effects the most important of which is gravitational light bending.

As an example, if the source height is small (of the order of few gravitational radii) a large fraction of the emitted photons is bent towards the disc by the strong gravitational field of the BH enhancing the illuminating continuum and strongly reducing the PLC at infinity, so that the spectrum is reflection–dominated. If the source height increases, gravitational light bending is reduced so that the observed PLC increases. Finally, if the height is very large so that light bending has little effect, the standard picture of reflection models with approximately half of the emitted photons being intercepted by the disc and the remaining half reaching the observer as the PLC is recovered.

With this setup, we compute the PLC and Fe line flux (representative of the whole RDC) as a function of the primary source height above the disc (see Miniutti et al 2003; Miniutti & Fabian 2004 for more details). Our results are presented in the left panel of Fig. 11 for the case of an accretion disc seen at an inclination of $30°$ (the relevant case for MCG–6-30-15). The black dots indicate different values for the source height ($h = 1, 5, 10, 20$ r_g from left to right). What the figure shows is that, once general relativistic effects are properly accounted for, the broad Fe line (and RDC) is not expected to respond simply to the observed PLC variation anymore. Three regimes can be identified (I, II, and III in the figure). A correlation is seen only in regime I, where the primary source height is between about 1 and 3–4 r_g. On the other hand, if the primary source has a height between about 4 r_g and 12 r_g (regime II) the broad Fe line (and RDC) variability is confined within 10 per cent only, while the PLC can vary by a factor ~ 4. We recall here that the observed variability of the RDC in the 2001 *XMM-Newton* observation is confined within 25 per cent despite variations by a factor 3–4 in the PLC.
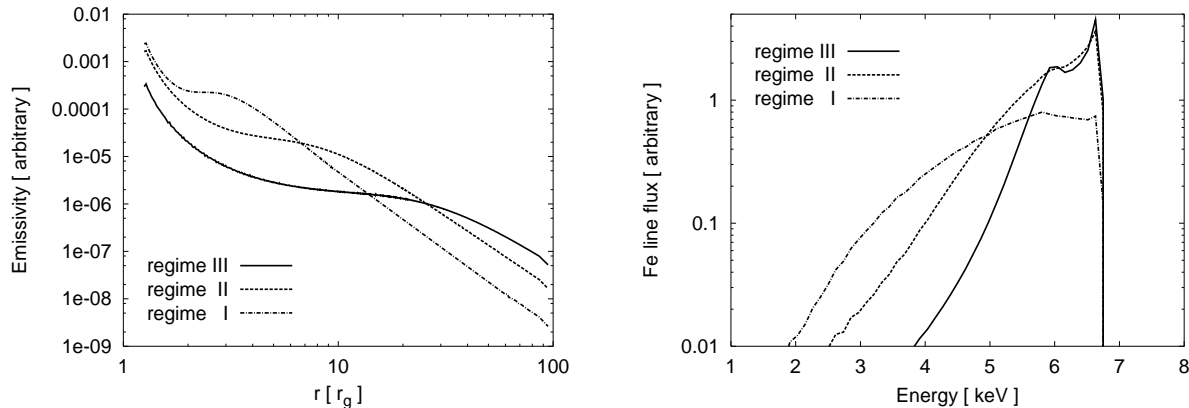
Figure 12: *Left panel*: Typical emissivity profiles computed in the light bending model for the three relevant regimes. The emissivity is steeper in the inner part of the disc and flattens outwards. *Right panel*: Typical line profiles in the three regimes. A log scale is used to enhance the line profile differences.

In the right panel of Fig. 11 we show the value of the reflection fraction predicted by the model as a function of the source height. When the source height is large, the standard value $R = 1$ is recovered. However, as the height decreases, light bending comes into play increasing the number of photons bent towards the disc while simultaneously reducing the number of those able to escape from the gravitational attraction. Thus, the reflection fraction increases dramatically. Two cases are shown in the figure, one for a source on the disc axis (solid), one for a ring–like configuration at $2\,r_g$ from the black hole axis. Regime II, which seems most relevant so far, is characterised by $R \simeq 2$. Quite remarkably this is precisely the measured value in MCG–6-30-15 during the simultaneous *XMM-Newton–BeppoSAX* 2001 observation we are discussing here.

Thus, if our model is qualitatively correct, it implies that MCG–6-30-15 was observed in regime II by *XMM-Newton* during the 2001 observation with most of the accretion power being dissipated within $5\,r_g$ in radius and in the range 4–$12\,r_g$ in height above the disc. This is itself a remarkable result implying that we are looking down to the region of spacetime where General Relativity exhibits itself at its best. Since the model computes self–consistently the disc illumination, the emissivity profile can be computed. In regime II, it turns out to be best described by a broken power law, very steep in the innermost region of the disc and flattening outwards, as observed in MCG–6-30-15 (see left panel of Fig. 12). We computed fully relativistic line profiles with our model and compared them with the data (Fig. 12, right panel). The line profiles obtained from regime II provide a very good match to the *XMM-Newton* data (Miniutti et al 2003).

As is clear from Fig. 11 (left panel), the model predicts a correlation between RDC and PLC at low flux levels. Fortunately, the *XMM-Newton* 2000 observation (that we did not discuss so far) caught MCG–6-30-15 in a slightly lower flux state than the 2001 one. The flux state is not remarkably lower, but some indications of the general behaviour can still be inferred. The details of the spectral analysis of the 2000 observation can be found in Wilms et al (2001) and Reynolds et al (2004). Here we only focus on the variability of the two components. If the source did not change dramatically its properties between the two observations, we should observe a somewhat correlated variability between the RDC and the PLC. A comparison between the two observations in this sense is shown in Fig. 13 where results of spectral analysis performed on 10 ks chunks for both observations are presented. In the right panel, the PLC slope Γ and RDC normalization are shown as a function of the PLC normalization for the higher flux 2001 *XMM-Newton* observation. The relevant panel is the bottom one showing the constancy of the RDC despite the large PLC variation. In the right panel of the same figure, we show the RDC vs. PLC
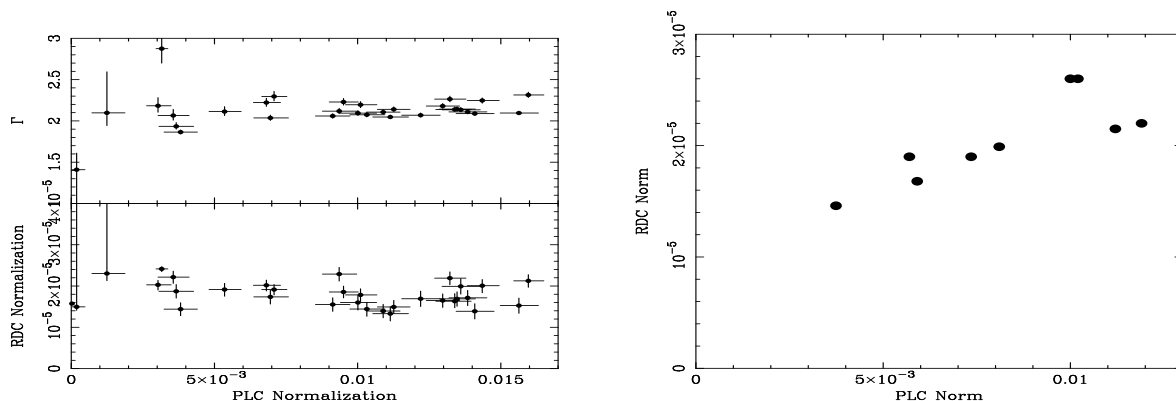
Figure 13: *Left panel*: PLC photon index (top) and RDC normalization as a function of the PLC normalization for the 2001 observation. *Right panel*: RDc normalization as a function of the PLC normalization for the 2000 *XMM-Newton* observation.

normalization for the lower flux 2000 *XMM-Newton* observation. As already reported by Reynolds et al (2004), a clear correlation is seen between the two components in this lower flux observation. This result was not known yet when the light bending model was being developed and provides unexpected support for the overall picture, matching one of the main predictions of the model.

The puzzling variability of the RDC and PLC, the large value of the reflection fraction, and even the emissivity and line profiles all seem to indicate the relevance of the light bending model for MCG–6-30-15. Given the very strong case for Fe line emission from the relativistic region in MCG–6-30-15, it would be a rather surprising coincidence if strong relativistic effects were not responsible for some, if not all, of the behaviour discussed above. We conclude by stressing that in all cases in which broad Fe lines are detected strong relativistic effects on the X–ray emission and variability cannot be ignored and have to be included in theoretical models. The light bending model is probably crude and incomplete, but represents a first significant step in this direction.

4.4 Occasional Fe line variability

As mentioned, the RDC and broad Fe line in MCG–6-30-15 is almost constant despite large variation in the PLC. However, it exhibits occasionally marked variations in the line profile such as during the 1994 *ASCA* observation (Iwasawa et al 1996b). Spectra were extracted in a high, medium, and very low flux state, the difference in count rate between the low and high flux being about a factor 4. The resulting line profiles are shown in the left panel of Fig. 14 where, from top to bottom, the line profile is for the high, medium and low flux state respectively. The general trend appears to be that the line is more peaked in high than low flux states and becomes much broader as the flux decreases. In particular, in the lowest flux state, no peak is visible at 6.4 keV and the line is very broad and redshifted. During the so–called deep minimum (bottom–left panel in Fig.14) the best–fitting parameters for the line profile indicate that emission is coming from within 6 r_g providing the first evidence for the presence of a Kerr BH in MCG–6-30-15, later confirmed by higher quality *XMM-Newton* data.

In the framework of the light bending model, low flux states correspond to situations in which the primary source is very close to the BH thereby illuminating very efficiently the inner disc. In higher flux states, the source has a larger height, and the outer disc starts to be illuminated as well. Therefore, the model predicts very broad and redshifted lines in low flux states (see also Fig. 12, right panel) while a peak at 6.4 keV due to emission from the outer regions of the disc appears at higher flux levels. In the right panel of Fig. 14 we show three profiles obtained in the light bending model for three different heights
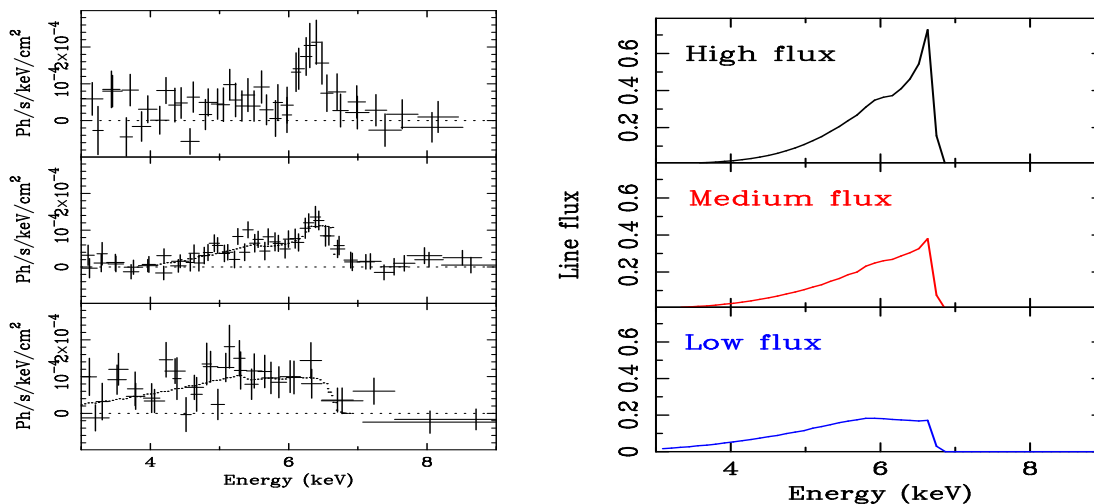
Figure 14: *Left panel*: The observed variations of the line profile during the 1994 *ASCA* observation (Iwasawa et al 1996). From top to bottom the high, medium, and low flux states profiles are shown. *Right panel*: The changes in the line profile predicted by the light bending model for the observed flux states.

of the primary source ($h = 6, 4, 2\ r_g$ from top to bottom). The profiles match the observed data rather well. It should be stressed that the PLC variation between $h = 2\ r_g$ (low flux) and $h = 6\ r_g$ (high flux) is predicted to be a factor 5, very similar to the factor 4 of the data.

Further remarkable evidence for variability of the Fe line on short–timescales is provided by the 1997 *ASCA* observation (Iwasawa et al 1999). During a bright flare, the Fe line profile changed dramatically. This is shown in Fig. 15 where the light curve and line profiles in two relevant time–intervals are shown. One possibility to explain such dramatic change is that a bright corotating flare appeared at about $5\ r_g$ from the BH. Given the low BH mass in MCG–6-30-15 (about $10^6\ M_\odot$) the flare has enough time to complete more than one orbit during the time–interval 'a', therefore resulting effectively in a ring–like emitting structure which provides a good fit to the data (Iwasawa et al 1999).

5   Other AGN: Seyfert1 and NLS1 galaxies

The case for a broad relativistic Fe line is very strong in MCG–6-30-15. In this source, the best–fitting parameters imply that Fe has about three times the solar abundance, the disc is lowly ionized, and the RDC is particularly strong with respect to the PLC ($R \simeq 2.2$). These conditions make it easier to detect the relativistic line in this AGN than in others. Indeed, it should be stressed that if these conditions were not met in MCG–6-30-15, the detection of a relativistic Fe line would be much more difficult, challenging present X–ray observatories. A discussion on the detectability of broad Fe line in less favourable conditions is deferred to Section 7 below.

Here we just show another interesting case of a broad Fe line, presented in Fig. 16. In the left panel, we plot the ratio of the *XMM-Newton* data of IRAS 18325–5926 with respect to a power law model fitted in the 2–10 keV band. The Fe line in IRAS 18325–5926 is clearly broad and exhibits a strong red wing extending down to about 4 keV (Iwasawa et al 1996a, Iwasawa et al 2004; Iwasawa et al, in preparation). Some other AGN in which resolved Fe lines have been reported in the past are discussed in Nandra et al (1997a,b; 1999); Bianchi et al (2001); Lamer et al (2003); Longinotti et al 2003; Balestra et al (2004); Porquet et al (2004b); Jiménez–Bailón et al (2005), the list being non–exhaustive. Some of the Fe lines in
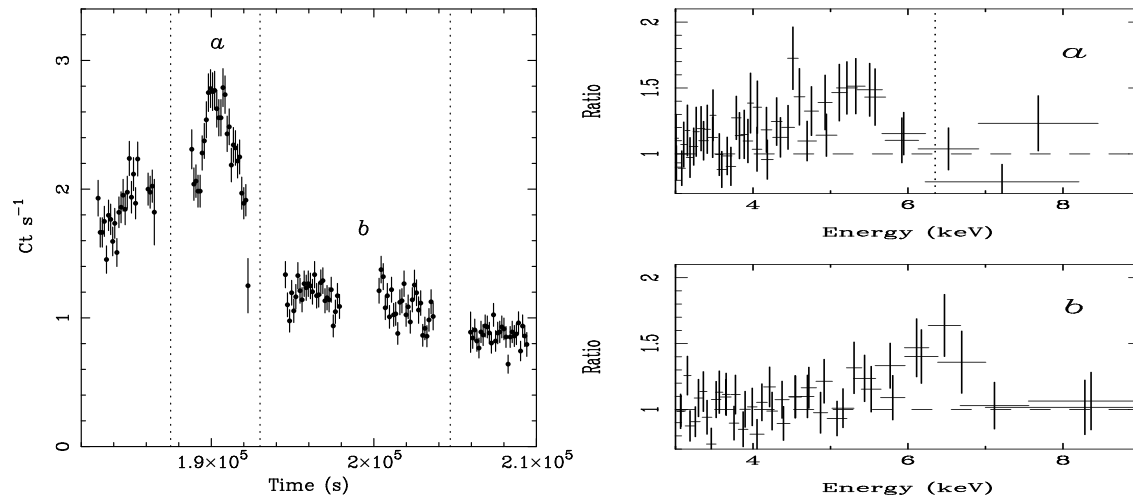
Figure 15: *Left panel*: The *ASCA* light curve around the bright flare (Iwasawa et al 1999). The two time–intervals relevant for the right panel of the figure are here defined. *Right panel*: During the flare (a) the broad line is redshifted well below the Fe Kα rest–frame energy (6.4 keV, vertical line). When the flare ceased (b) the broad line recovered to the ordinary profile.
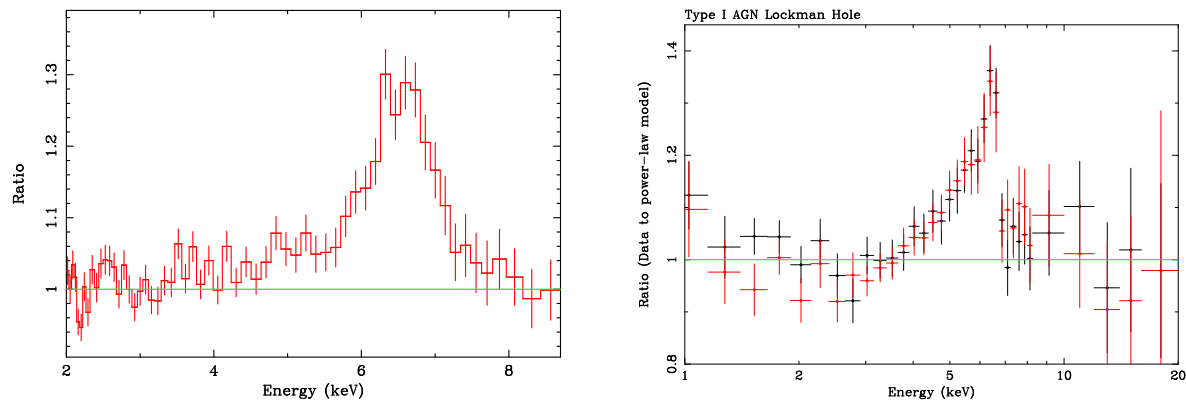
Figure 16: *Left panel*: Ratio of the spectrum of IRAS 18325–5926 to a power law for *XMM-Newton* data. *Right panel*: Ratio plot of the mean unfolded spectrum for type–1 AGN in the Lockman Hole with respect to a power law (Streblyanska et al 2005). *XMM-Newton* EPIC–pn and MOS detectors are used.

the list are not extreme and do not imply that the reflector extends down below the ISCO of a non–rotating BH, thereby not constraining the BH spin. The line width in these objects is however inconsistent with emission from a very distant reflector such as the torus and/or the Broad Line Region and seems often inconsistent with being a blend of numerous narrower lines.

It should be stressed that not all broad lines are clear and unambiguous as in MCG–6-30-15, and other interpretations of the data are often possible. A possible scenario is that complex absorption by large columns of highly ionized matter produces a curvature in the spectrum that resembles that of a broad Fe line (e.g. Turner et al 2005). As mentioned, this was conclusively excluded for MCG–6-30-15 but is a possible alternative to relativistic lines in other cases. The recently launched Astro–E2 mission has enough effective area and energy resolution in the relevant Fe band to test this scenario by detecting or not the absorption features associated with it. High energy data will also be crucial because they can indicate the presence/lack of strong reflection components through the detection of the Compton hump therefore suggesting which interpretation is preferable.

The 770 ks *XMM-Newton* observation of the Lockman Hole field provides also some interesting information. The Lockman Hole is a special field in the sky because of extremely low Galactic absorption. It is therefore an ideal field to study faint AGN as a population and their contribution to the X–ray background. The field comprises 53 type–1 and 41 type–2 AGN with known redshifts. Streblyanska et al (2005) have obtained the mean spectrum of type–1 AGN by stacking together the individual spectra and correcting for the source redshift (see also Brusa et al 2005 for a spectral stacking results from the Chandra Deep Fields). The ratio of the data to a power law model for the mean type–1 AGN spectrum is shown in the right panel of Fig. 16 and exhibits a broad emission feature peaking at 6.4 keV. A prominent broad red wing is also visible. The observed equivalent width is larger than the average value for bright nearby Seyfert 1 galaxies but similar for example to MCG–6-30-15 and might indicate that Fe is overabundant with respect to solar values. Shemmer et al (2004) have suggested that the metallicity in AGNs is correlated with the mass accretion rate (close to the Eddington limit), which is in turn related to the AGN luminosity. It is possible that the large equivalent widths measured here are due to high metallicity in distant and luminous objects. The average line profile is best–fitted with an inner disc radius of 3 r_g. This may be an indication that most of the AGNs contain a Kerr BH at their very centre which would have serious implications for the dominant BH growth mechanisms and, more broadly, on cosmology and galaxy evolution.

5.1   1H 0707–495: a key to the nature of NLS1?

Narrow Line Seyfert 1 galaxies tend to show steep soft X-ray spectra, extreme X–ray variability, and sometimes broad iron emission features. One extreme such object is 1H 0707-495 which has a marked drop in its spectrum above 7 keV. This is either an absorption edge showing partial-covering in the source (Boller et al. 2002; Gallo et al 2004; Tanaka et al 2004) or the blue wing of a massive, very broad, iron line (Fabian et al. 2002b, 2004). Here we explore in some detail this latter possibility as an example of what could be a more general picture relevant to many other objects. 1H 0707–495 has been observed twice by *XMM-Newton* with a deep spectral drop at 7 keV discovered in the first observation. The drop had shifted to 7.5 keV in the second observation two years later.

In the left panel of Fig. 17 we show the ratio of the data (second observation) to a simple power law model fitted between 2 and 4 keV and above 7.5 keV. A large skewed emission feature is seen, very similar to that of MCG–6-30-15 (see the right panel of Fig. 8) together with a steep soft excess below 1–2 keV. We have fitted the broadband 0.5–10 keV spectrum with a simple two–component model comprising a PLC and a relativistically blurred RDC obtaining an excellent description of the entire data set. The data require Fe to have super–solar abundance (3 times the solar value) and the reflector to be ionized at the level of $\xi \simeq 650$ erg cm s^{-1}. The X–ray reflection spectrum comes from the innermost regions of the disc
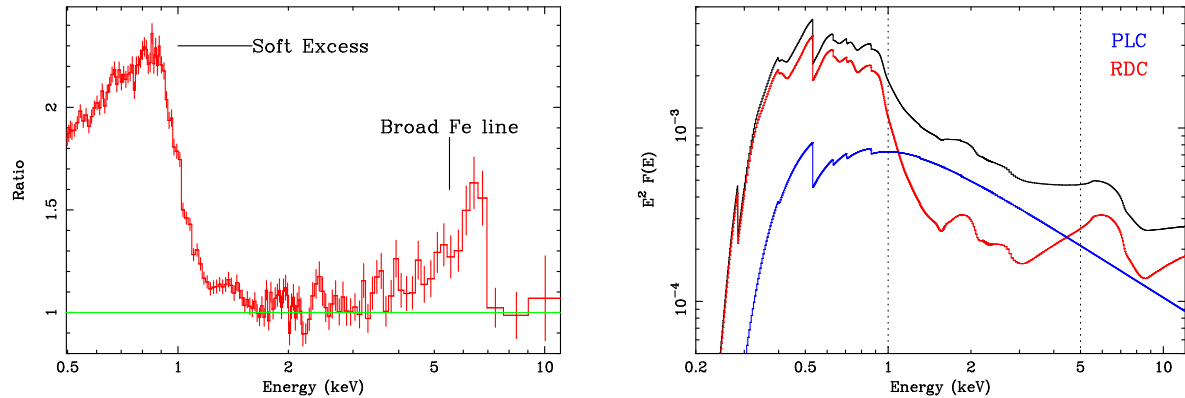
Figure 17: *Left panel*: Ratio of the spectrum of the NLS1 1H0707 to a power-law fitted between 2 and 4 keV and above 7.5 keV. *Right panel*: Spectral decomposition of 1 H0707–495 in terms of a variable power-law (blue) and a blurred reflection component (red). Vertical lines separate the regions in which one of the two components dominates the spectrum.
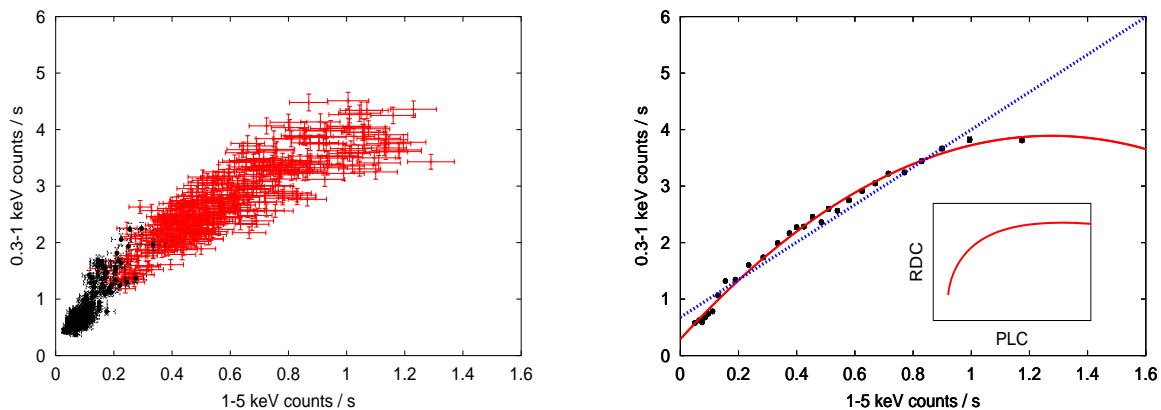

Figure 18: *Left panel*: Flux–flux plot for the two observations of 1H 0707–495. The 0.3–1 keV band is representative of the RDC, whereas the 1–5 keV band of the PLC (see right panel of Fig. 17). *Right panel*: Binned version of the flux–flux plot. A linear relation is a much worse fit than a curved one. In the insert panel, we show the prediction of the light bending model.

with inner disc radius measured at 2.3 r_g and steep emissivity profile (Fabian et al 2004). In comparison, the emissivity was even steeper during the first observation which explains why the marked spectral drop (that we interpret as the combination of the reflection edge and blue peak of the Fe line) was at lower energy (7 keV in the first and 7.5 keV in the second observation). The shift is due to gravitational redshift which is more effective in lowering the energy of sharp features when the emissivity is steeper (i.e. the first observation).

The best–fit model is shown in the right panel of Fig. 17. The solution implies that the spectrum is almost completely reflection–dominated, i.e. the PLC illuminates much more efficiently the disc than the observer at infinity. This seems therefore to be a promising source in which to test further the light bending model that successfully reproduces the spectral shape and variability of the key source MCG–6-30-15. In fact the model predicts the existence of reflection–dominated states in regime I and part of regime II.

From the right panel of Fig. 17, the RDC dominates the spectrum below about 1 keV and above 5 keV, whereas the PLC dominates in the intermediate 1–5 keV band (the vertical lines in the figure separate the different energy bands). As a zeroth–order approximation, we can then consider the 1–5 keV flux as representative of the PLC, while the 0.3–1 keV flux is associated with the RDC. If so, by plotting the 0.3–1 keV count rate as a function of the 1–5 keV one, we could infer the RDC correlation with the PLC.

This is shown in the left panel of Fig. 18 for both the first (black) and second (red) observations. There is clearly a correlation that, however, is not linear. This is more clearly shown in the binned version of the same plot, showed in the right panel of Fig. 18. The correlation is non–linear, and a curved relationship is preferred by the data. In the insert, we show the prediction of the light bending model which seems to catch the overall behaviour surprisingly well. The insert is appropriate for an accretion disc seen at $30°$, while the disc inclination in 1H 0707-495 is likely more $50°$. As shown in Miniutti & Fabian (2004) the light bending model predicted behaviour for larger inclination is even more similar to that seen in the data.

We conclude by noting that, quite remarkably, a relativistically blurred reflection-dominated model describes well the XMM-Newton spectrum of 1H 0707-49 over the entire observed energy band (for both observations). Strong gravitational light bending around a Kerr BH seems to be the simplest explanation for the peculiar spectrum of this source and its remarkable variability. More detailed analysis of the data sets is given in Fabian et al (2002b; 2004) where further support in favour of the light bending model is given. The same scenario described above is also relevant for 1H 0419-577 (Fabian et al 2005) and NGC 4051 (Ponti et al 2005). An alternative description in terms of partial covering is provided by Boller et al (2002); Gallo et al (2004); Tanaka et al (2004). See also Pounds et al (2004a) for a similar partial–covering interpretation of the low flux state of 1H 0419–577.

6   Galactic Black Holes Candidates

Black hole binaries are accreting systems containing a dark compact primary with a mass larger than about $3\,M_\odot$ and a non–degenerate companion. These are generally refereed to as confirmed BH binaries because the high mass of the primary excludes it is a neutron star. Only 18 such systems are known in our Galaxy, but they are thought to be representative of a large population of systems (possibly around 30 millions of sources). The first to be discovered was Cyg–X1, containing a BH of 6.9–13.2 $M_\odot$ with a O/B star as companion. In addition, many other X–ray sources in the Galaxy do exhibit all the observed characteristics of BH binaries. Many of these sources can not be claimed as secure BH binaries because the mass of the primary is not well constrained, and they are generally referred to as Galactic BH Candidates (GBHCs).

BH binaries and GBHCs exhibit a fascinating phenomenology which manifest itself in complex X–ray spectral and temporal properties. In many respects, these sources can be thought as scaled–down versions of AGN both powered by accretion into the central BH. It is not our purpose here to explore the complexity of BH binaries and GBHCs, and we refer the interested reader to more specialistic reviews such as, for example, the one by McClintock & Remillard (2004). Our interest here is to focus on the broad relativistic Fe lines that have been detected in many objects, sometimes suggesting that the central BH is rapidly spinning. One such a case, the GBHC XTE J1650–500, will be presented in some detail, mainly because its 2001 outburst was covered by three different X–ray detectors (*RXTE*, *BeppoSAX*, *XMM-Newton*) and is therefore particularly well characterized (though this is clearly not the only source which benefits from such an extensive X–ray coverage).

Examples of broad Fe lines detected with *ASCA* in the X–ray spectra of GBHcs are shown in the left panel of Fig. 19 from Miller et al (2004). Other broad lines have been found in other GBHCs, especially in the high and very high/intermediate states where the accretion disc is believed to extend down to small radii (Martocchia et al 2002; Miller et al 2002a,b,c; 2003). In the right panel of the same Figure, we show the *XMM-Newton* Fe line profile of GX 339–4 (Miller et al 2004b). A similar profile is detected by *Chandra* as well (Miller et al 2004a).
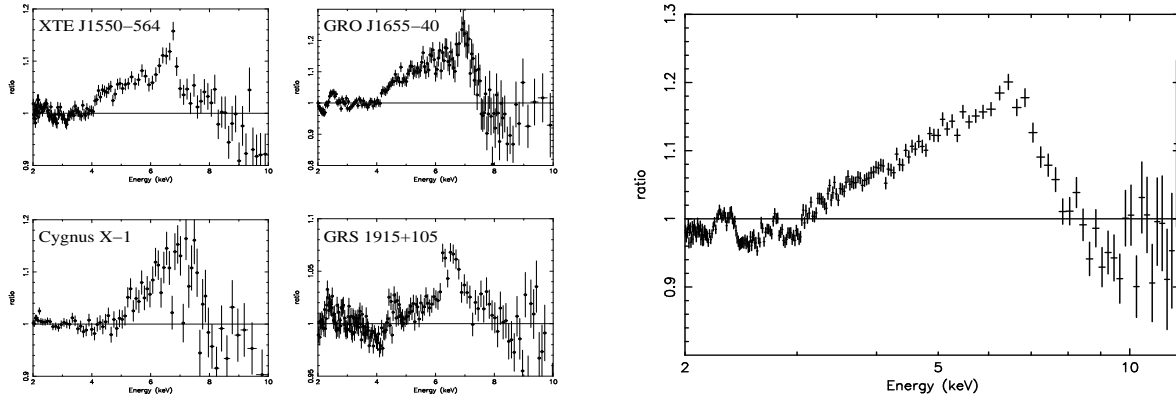
Figure 19: *Left panel*: Prominent relativistic lines observed with *ASCA* in GBHC. When fitted with relativistically blurred reflection models all sources but GRS 1915+105 require emission from within the ISCO of a non–rotating BH, suggesting that the BHs in most sources are rapidly spinning. *Right panel*: The broad iron line in GX 339–4 as observed by *XMM-Newton* (Miller et al 2004b).
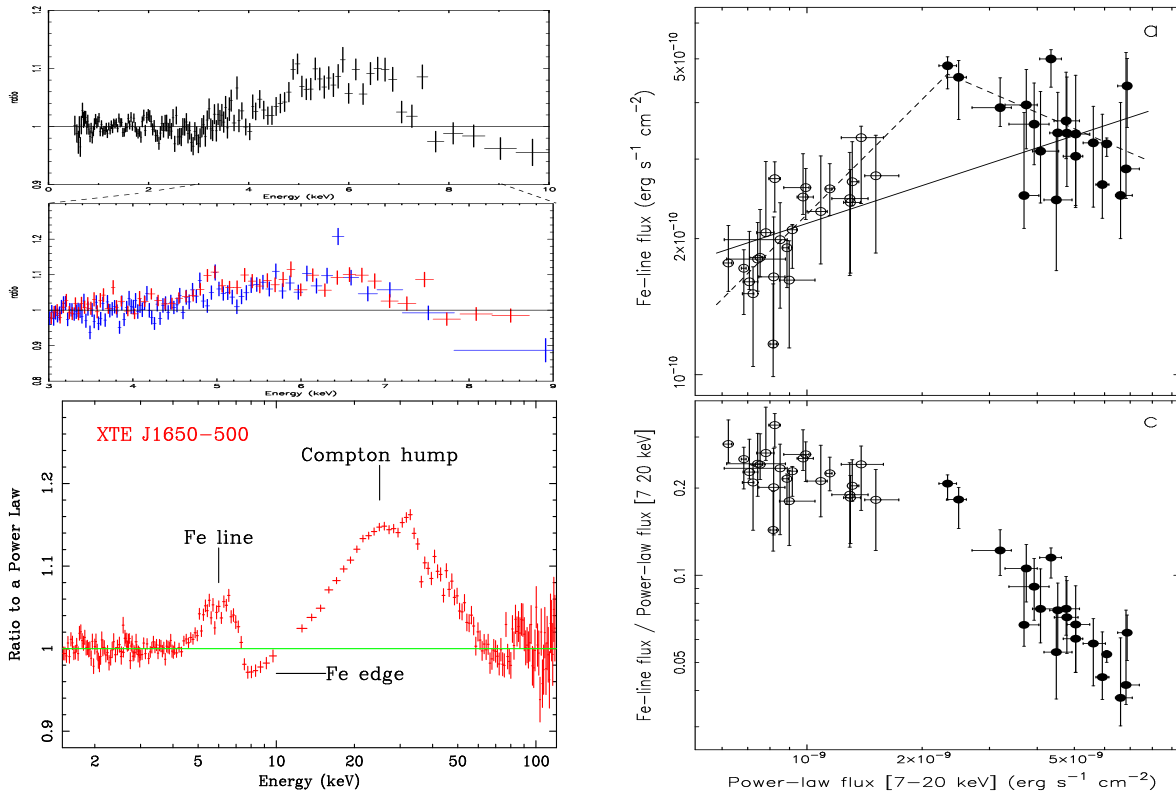

Figure 20: *Left–top panel*: The line profile of XTE J1650–500 as observed with *XMM-Newton* (Miller et al 2002a). *Left–middle panel*: Superposition of the broad lines in XTE J1650–500 (red) and Cyg X–1 (blue) from Miller et al 2002a. *Left–bottom panel*: Broadband *BeppoSAX* spectrum of XTE J1650–500 (as a ratio to the continuum). The signatures of relativistically–blurred reflection are clearly seen. *Rigt–top panel*: The broad Fe line flux is plotted versus the ionizing continuum. *Right–bottom panel*: The ratio between the line flux and the continuum (i.e. a measure of the reflection fraction) is plotted against the ionizing flux. Both right panels are from Rossi et al (2005) and refer to *RXTE* data.

6.1   The case of XTE J1650–500

XTE J1650–500 is a X–ray binary with a period of about 7.6 hours and an optical mass function $f(M) = 2.73 \pm 0.56 \ M_\odot$. If typical mass ratios with the companion and an inclination of about $50°$ are assumed (the latter in agreement with X–ray spectroscopy) the mass of the primary turns out to be $7.3 \pm 0.6 \ M_\odot$ strongly suggesting the presence of a central BH (Orosz et al. 2004). The source outburst was followed up during 2001 by *BeppoSAX* (three observations) *XMM-Newton* (one observation) and *RXTE* itself (57 pointed observations). The *XMM-Newton* observation revealed the presence of a broad relativistic line (Miller et al 2002a) which is shown in the top–left panel of Fig. 20. The line profile extends down to about 4 keV and implies emission from within the ISCO of a non–rotating BH. An inner disc radius at the ISCO of a Maximal Kerr hole ($\simeq 1.24 \ r_g$) is prefered over one at the ISCO of a Schwarzschild BH at the 6σ level, strongly suggesting that the BH is rapidly, possibly maximally, spinning. The emissivity profile is much steeper than standard and implies that energy dissipation preferentially occurs in the inner few r_g from the center.

   The source was observed three times by *BeppoSAX* and in all cases a broad relativistic Fe line was detected confirming the main results of Miller et al (2002a) with respect to both inner disc radius and steep emissivity (Miniutti, Fabian & Miller 2004). The broadband coverage provided by *BeppoSAX* (up to 200 keV) allowed us to detect the large reflection hump around 20–30 keV which is the unambiguous sign of the presence of a X–ray reflection spectrum, associated with the broad Fe line, giving more strength, if necessary, to the interpretation of the broad spectral feature as a relativistic Fe line. The broadband spectrum during one of the *BeppoSAX* observations is shown in the bottom–left panel of Fig. 20 as a ratio with a power law (and soft thermal emission) model.

   The steep emissivity profile and small inner disc radius are very reminiscent of the case of MCG–6-30-15. In the latter case, the variability of the Fe line was succesfully explained by the light bendind model. It is therefore an interesting exercise to study the Fe line variability in XTE J1650–500 as well and to put to test the light bending model not only in AGNs, but in GBHCs as well. The three *BeppoSAX* observations already gave some indication in that direction (Miniutti, Fabian & Miller 2004) suggesting the relevance of the light bending model for this object. Further study by Rossi et al (2005) confirmed the first indication in a quite spectacular way. By using the 57 pointed observation by *RXTE*, Rossi et al studied the broad Fe line variability in detail during the outburst. The results of their analysis is shown in the right panels of Fig. 20. The Fe line flux is correlated with the power law continuum at low fluxes and then saturates (or even shows some marginal evidence for anti–correlation) at higher flux levels. Its ratio with the power law continuum flux (a proxy for the reflection fraction) is generally anti–correlated with the continuum and saturates only at low fluxes. Those two results match very well the predictions of the light bending model (see e.g. Fig.11). We therefore suggest that during the 2001 outburst of XTE J1650–500 most of the primary emission comes from a compact corona (or the base of a jet) located within the innermost few r_g from the BH and that strong gravitational light bending is responsible for most of the observed variability, as in MCG–6-30-15.

7   Broad-line-free sources and nature of the soft excess

A broad relativistic Fe line is present in some but not all AGN spectra. On the other hand *XMM-Newton* and *Chandra* have shown that a narrow Fe line is almost ubiquitous in the X–ray spectrum of Seyfert galaxies (e.g. Page et al 2004; Yaqoob & Padmanabhan 2004). The narrow line is generally interpreted as due to reflection from distant matter (at the parsec scale or so) such as the putative molecular torus, in good agreement with unification schemes. Here we explore in some detail some of the possible explanations for the non–ubiquitous detection of relativistic broad lines in sources that are expected to be radiatively

efficient and, according to the standard model, should have an accretion disc extending down to small radii and therefore a broad Fe line as well.

7.1   Observational limitations

The X–ray spectrum of Seyfert 1 and NLS1 galaxies and quasars is characterised by the presence of a narrow Fe line and by a soft excess, i.e. soft excess emission with respect to the 2–10 keV band spectral shape. The soft excess is often interpreted as thermal emission from the accretion disc. However, this interpretation is somewhat controversial. For example, Gierlinski & Done (2004) have selected a sample of 26 radio–quiet PG quasars for which good–quality *XMM-Newton* observations are available and tried to characterise their soft excesses. When interpreted as thermal emission, the soft excess in the sample has a mean temperature of 120 eV with a very small variance of 20 eV only. On the other hand, the maximum temperature of a standard Shakura–Sunyaev disc depends on the BH mass and on the mass accretion rate, which can in turn be related to the ratio between disc luminosity and Eddington luminosity as $T_{\max} \propto M_{\mathrm{BH}}^{-1/4}(L_{\mathrm{disc}}/L_{\mathrm{Edd}})^{1/4}$. For the BH masses and luminosities of the PG quasars in the Gierlinski & Done sample, one would expect temperatures in the range 3–70 eV. Thus two problems arise: i) the measured temperature of the soft excess is too uniform in sources that exhibit large differences in BH mass and luminosity; ii) the measured temperature is by far too high with respect to that predicted from standard accretion disc models. The uniformity of the soft excess spectral shape (and therefore of the inferred temperatures) was noted before by e.g. Walter & Fink (1993) and Czerny et al (2003).

The uniformity and implausibly high temperature of the soft excess raises the question on the true nature of the soft excess. A uniform temperature could be easily understood if the soft spectral shape was due to atomic rather than truly thermal processes, the obvious candidate being ionized reflection from the disc. The uniformity and too large temperature of the soft excess may be then the result of applying the wrong spectral model (thermal emission) to the data. When a broad Fe line is present (e.g. MCG–6-30-15, 1H 0707–495) the parameters of the reflection and relativistic blurring are all constrained by the line shape and energy. It is then remarkable that the same model, once extrapolated in the soft band, provides an excellent description of the broadband spectrum and does not need any additional soft excess. We therefore suggest that relativistically blurred ionized reflection may well be responsible for the soft excess in many other objects as well (see also Ross & Fabian 2005; Crummy et al, in preparation).

We then construct a theoretical model for what we believe could well be the typical X–ray spectrum of radiatively efficient X–ray sources. The model comprises a power law component and reflection from distant matter (represented by neutral reflection continuum and narrow Fe line). The soft excess is provided by ionized reflection from the accretion disc that also contributes to the hard band mainly with a broad relativistic line. We assume solar abundances and isotropic illumination of the accretion disc with reflection fraction $R \sim 1$. These conditions are less favourable for the detection of the relativistic Fe line than those found for example in MCG–6-30-15 and 1H 0707–495, in which the Fe abundance is super–solar and the RDC contribution particularly high, and should represent the typical and most common situation. The ionized reflection spectrum is convolved with a Laor model reproducing the Doppler and gravitational effects in an accretion disc around a Maximal Kerr BH (the other parameters being the disc inclination and the emissivity index, chosen to be $i = 30°$ and $q = 3$).

The model is shown in the top–left panel of Fig. 21: a flux of 3×10^{-12} erg cm^{-2} s^{-1} in the 2–10 keV band is assumed. We then simulated an *XMM-Newton* observation with a typical exposure time of 30 ks. The simulated spectrum is shown in the top–right panel of Fig. 21 as a ratio with a power law in the 2–10 keV band. The main features in the simulated spectrum are a narrow 6.4 keV Fe Kα line and a soft excess below 1–2 keV, as generally observed in Seyfert galaxies and quasars. The broad Fe line is completely lost into the continuum and no detection can be claimed with any significance. In
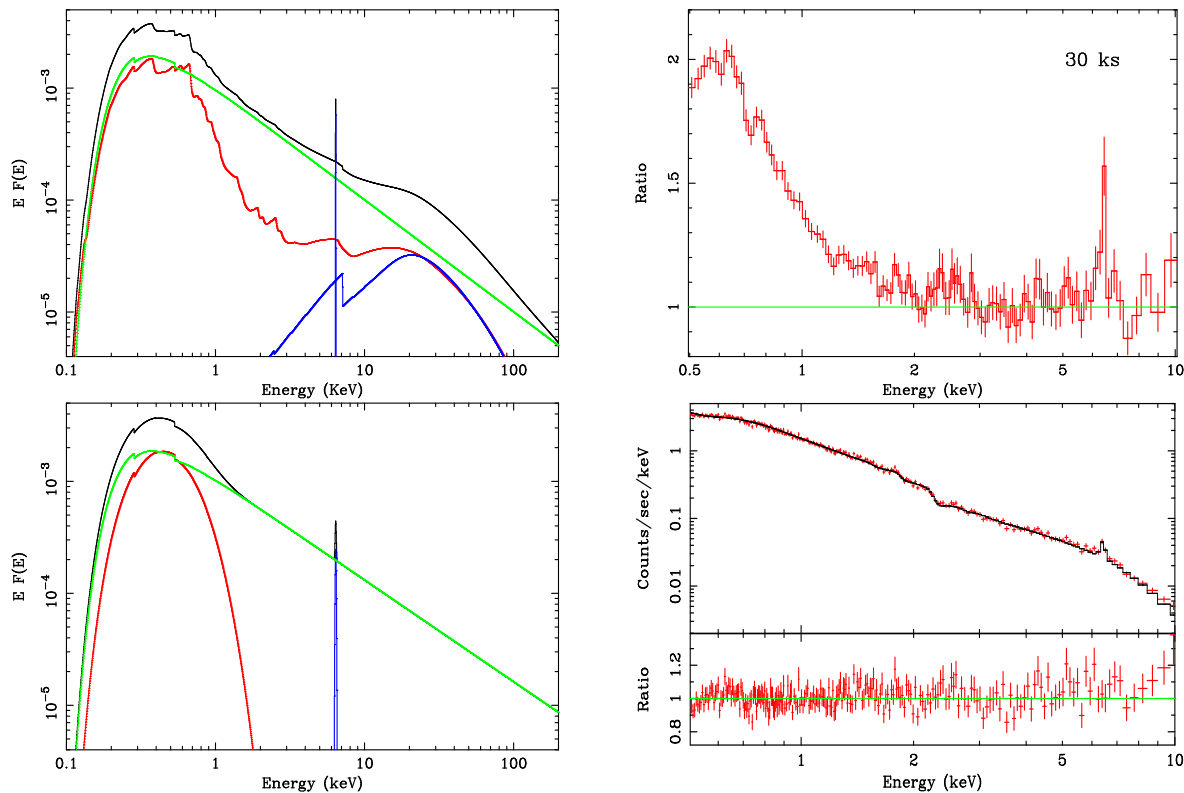
Figure 21: *Top–left panel*: The model we assumed for the simulations, based on our experience with X–ray data of Seyfert 1 and NLS1 galaxies. *Top–right panel*: 30 ks *XMM-Newton* simulated spectrum with the model shown in the top–left panel as a ratio with a power law fitted in the 2–10 keV band. The only prominent features are a narrow 6.4 keV Fe line and a steep soft–excess below about 1–2 keV, as generally observed. *Bottom–left panel*: The "standard model" that is often used to fit the X–ray spectra of Seyfert 1 and NLS1 galaxies. *Bottom–right panel*: The 30 ks *XMM-Newton* simulated spectrum is fitted with the "standard model" shown in the bottom–left panel. The fit is excellent with reduced χ^2 of 0.98.

fact, the spectrum can be described by the generally adopted model (hereafter "standard model") shown in the bottom–left panel of Fig. 21 comprising a power law, narrow Fe line, and blackbody emission to model the soft excess. The fit with this model is shown in the bottom–right panel of the same figure and is excellent. It should be noted that the measured temperature of the soft excess is $kT = 125 \pm 15$ eV, exactly in the range in which the "uniform temperature" of the soft excess is found.

The non–detection of the broad relativistic line is also very significant. This means that if the soft excess is due to ionized reflection from the disc, the associated broad Fe line cannot be detected with present–quality data unless some specific conditions are met such as high Fe abundance, large RDC contribution, etc. This would naturally explain not only the nature of the soft excess in many sources but also the reason why the broad relativistic line is not ubiquitously detected in radiatively efficient sources. In the future, when X–ray missions with much larger effective area at 6 keV will be launched (XEUS/Constellation–X) our interpretation can be tested against data. In Fig. 22 we show the same spectrum simulated for a 100 ks Constellation–X observation. In the left panel, we show the spectrum and the ratio with the "real model" (top–left panel of Fig. 21), while in the right panel, the fit is made by using the "standard model" (bottom–left of Fig. 21. The "standard model" clearly is an unacceptable fit to the data and leaves residuals throughout the observed band, most remarkably the broad Fe line between 4 keV and 7 keV as well as soft residuals due to unmodelled soft features in the reflection spectrum.
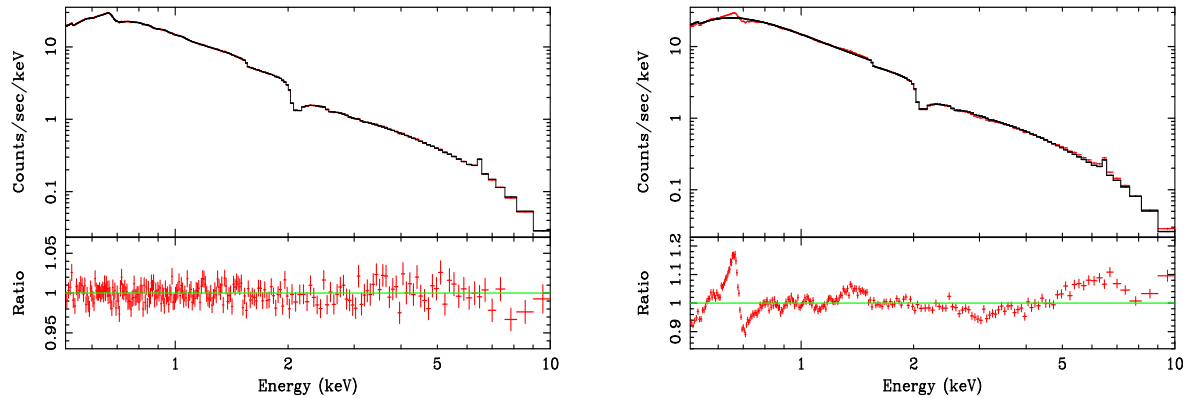
Figure 22: *Left panel*: 100 ks Constellation–X (or XEUS with similar results) simulated spectrum with the same model as for the 30 ks *XMM-Newton* simulation. *Right panel*: The Constellation–X simulated spectrum is fitted with the "standard model" The fit is now totally unacceptable. The broad Fe line is now clearly seen in the 4–7 keV band, and residuals corresponding to reflection features are left at all energy of the spectrum. Future large collecting area missions such as XEUS and Constellation–X will therefore be able to distinguish easily between the two proposed models.

7.2 Generalization of the light bending model

Good examples of broad–line–free sources from long *XMM-Newton* exposures (among others) are Akn 120, which has no warm absorber (Vaughan et al. 2004), the Seyfert 1 galaxy NGC 3783 (Reeves et al 2004), and the broad line radio galaxy 3C 120 (Ballantyne, Fabian & Iwasawa 2004). Various possibilities for the lack of any line have been proposed by the authors of those and other papers including: a) the central part of the disc is missing; b) the disc surface is fully ionized (i.e. the Fe is); c) the coronal emissivity function is flat, which could be due to d) the primary X-ray sources being elevated well above the disc at say $100r_{\mathrm{g}}$.

There are also intermediate sources where the data are either poor or there are complex absorption components so that one cannot argue conclusively that there is a relativistic line present. Some narrow line components are expected from outflow, warm absorbers and distant matter in the source. One common approach in complex cases, which is not recommended, is to continue adding absorption and emission components to the spectral model until the reduced χ^2 of the fit is acceptable, and then claim that model as the solution. Very broad lines are difficult to establish conclusively unless there is something such as clear spectral variability indicating that the power-law is free of Fe-K features, as found for MCG–6-30-15, or for GX 339-4 and XTE J1650–500 where the complexities of an AGN are not expected.

Our interpretation of the spectral behaviour of MCG–6-30-15 and some other sources means that we are observing the effects of very strong gravitational light bending within a few gravitational radii of a rapidly spinning black hole. The short term (10–300 ks) behaviour is explained, without large intrinsic luminosity variability, through small variations in the position of the emitting region in a region where spacetime is strongly curved. This implies that some of the rapid variability is due to changes in the source position. Now BHC in the (intermediate) high/soft state have high frequency breaks at higher frequency, for the same source, than when in the low/hard state (cf. Cyg X-1, Uttley & McHardy 2004). This additional variability when in the soft state could be identified with relativistic light-bending effects on the power-law continuum.

This picture suggests a possible generalization of the light-bending model to unify the AGN and GBHC in their different states. Note the work of Fender, Belloni & Gallo (2004) which emphasises that jetted emission occurs commonly in the hard state of GBHC. The key parameter may be the mean height of the main coronal activity above the black hole. Assume that much of the power of the inner disc passes

into the corona (Merloni & Fabian 2001a,b) and that the coronal activity is magnetically focused close to the central axis. Then at low Eddington ratio the coronal height is large (say $100r_g$ or more), the corona is radiatively inefficient and most of the energy passes into an outflow; basically the power flows into a jet. Reflection is then appropriate for Euclidean geometry and a flat disc and there is only modest broadening to the lines. If the X-ray emission from the (relativistic) jet dominates then X-ray reflection is small (see e.g. Beloborodov 1999). The high frequency break to the power spectrum is low ($\sim 0.001c/r_g$).

When the Eddington fraction rises above say ten per cent, the height of the activity drops below $\sim 20r_g$, the corona is more radiatively efficient and more high frequency variability occurs due to light bending and the turnover of the power spectrum rises above $0.01c/r_g$. The X-ray spectrum is dominated at low heights by reflection, including reflection-boosted thermal disk emission, and a broad iron line is seen. Any jet is weak. The objects with the highest spin and highest accretion rate give the most extreme behaviour. Observations suggest that these include NLS1 and some very high state, and intermediate state, GBHC. Some broad-line-free sources do not however fit this model, so more work is required also to match the observed timing properties and not only the spectral variability.

8   Short–timescale variability in the Fe K band

In addition to the major line emission around 6.4 keV, transient emission features at energies lower than 6.4 keV are sometimes observed in X-ray spectra of AGN. As discussed, an early example was found in the ASCA observation of MCG–6-30-15 in 1997, which was interpreted as Fe K emission induced from a localised region of the disc, possibly due to illumination by a flare above it (Iwasawa et al 1999, see Fig. 15). More examples followed in recent years with improved sensitivity provided by XMM-Newton and Chandra X-ray Observatory (Turner et al 2002; Petrucci et al 2002; Guainazzi et al 2003; Yaqoob et al 2003; Ponti et al 2004; Dovčiak et al 2004; Turner Kraemer & Reeves 2004; Longinotti et al 2004; Porquet et al 2004; Miniutti & Fabian 2005). These features can be attributed to an Fe Kα line arising from relatively localised reflecting spots on the accretion disc. If the spot is close to the central black hole, then the line emission is redshifted, depending on the location of the spot on the disc (Iwasawa et al 1999; Ruszkowski 2000; Nayakshin & Kazanas 2001; Dovčiak et al 2004). Here we present one case only, probably the most spectacular observed so far (NGC 3516, Iwasawa, Miniutti & Fabian 2004)

8.1   The remarkable case of NGC 3516

Iwasawa, Miniutti & Fabian (2004) selected one of the XMM-Newton observations of the bright Seyfert galaxy NGC3516, for which Bianchi et al (2004) reported excess emission at around 6 keV in addition to a stronger 6.4 keV Fe Kα line in the time-averaged EPIC spectrum and studied the short–timescale variability of the 6 keV emission feature. We consider the 5–7.1 keV band, free from absorption which can affect energies above and below and fit an absorbed power law model to the data. The only residual emission features in the time–averaged spectrum are then two relatively narrow emission lines at 6.4 keV and 6 keV (hereafter the "line core" and "red feature" respectively). This is shown in the left panel of Fig. 23 where the line(s) profiles detected in the time–averaged spectrum are plotted.

We first investigated the excess emission at resolutions of 5 ks in time and 100 eV in energy. A smoothed image of the excess emission in the time-energy plane is constructed from individual intervals of 5 ks. The detailed procedure of this method is described in Iwasawa, Miniutti & Fabian (2005). The light curves of the line core at 6.4 keV (6.2–6.5 keV) and of the red feature (5.8–6.2 keV) are obtained from the image and shown in the right panel of Fig. 23. The errors on the line fluxes are estimated from extensive simulations as discussed in Iwasawa, Miniutti & Fabian (2005). The red feature apparently shows a recurrent on-and-off behaviour which is suggestive of about four cycles with a timescale of 25 ks.
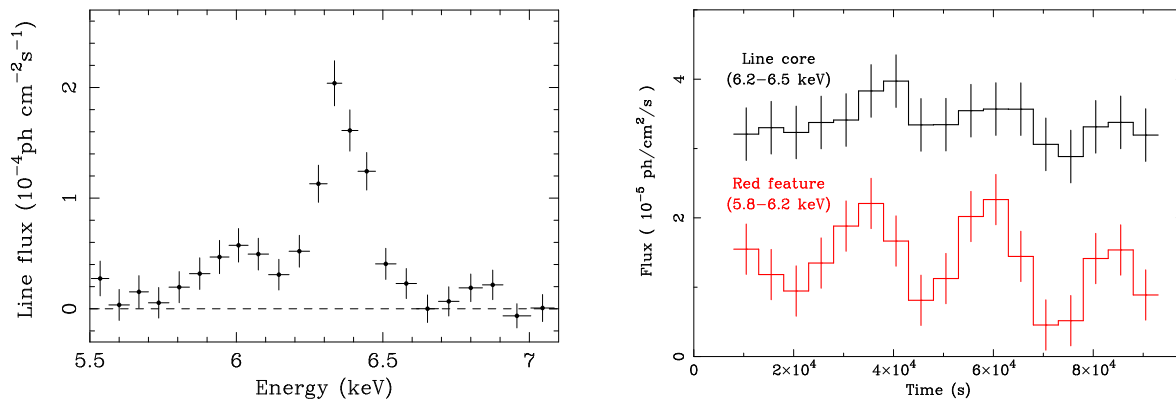
Figure 23: *Left panel*: Time–averaged line(s) profile of NGC 3516. Two major emission features are seen, namely a line core at 6.4 keV and a red feature around 6 keV (rest–frame). *Right panel*: Light curves of the line core and red feature on a 5 ks timescale. The red feature seems to vary on a characteristic timescale of 25 ks while the line core is largely constant, apart from a possible increase delayed from the 'on' phase in the red feature by a few ks.

In contrast, the 6.4 keV line core remains largely constant, apart from a possible increase delayed from the 'on' phase in the red feature by a few ks. Folding the light curve of the red feature confirms a characteristic interval of about 25 ks. The left panel of Fig. 24 shows the folded light curve of the red feature (red), as well as the one obtained from the original unsmoothed data (blue) by folding on a 25 ks interval.

Using the light curves as a guide (see right panel of Fig. 23), we constructed two spectra by selecting intervals in a periodic manner from the on and off phases to verify the implied variability in the red feature. The line profiles obtained from the two spectra are shown in the right panel of Fig. 24. The 6.4 keV core is resolved slightly ($\sim 5,000$ km s^{-1} in FWHM) and found in both spectra with an equivalent width of 110 eV. While the 6.4 keV core remains similar between the two, there is a clear difference in the energy range of 5.7–6.2 keV due to the presence/absence of the red feature. The variability detected between the two spectra is significant at more than the 4σ level.

We then investigated the variability of the red feature on shorter timescales to establish if not only flux, but also energy variation can be detected, with the ultimate goal of inferring the origin of the red feature. We constructed an image in the time–energy plane with 2 ks resolution in time and 100 eV in energy. The resulting image is seen in the left panel of Fig. 25 where the colour scale indicates the number of photons detected above the continuum (dark blue corresponding to about 15 counts). The image shows a relatively stable line core around 6.4 keV, while the red feature apparently moves with time during each on phase: the feature emerges at around 5.7 keV, shifts its peak to higher energies with time, and joins the major line component at 6.4 keV, where there is marginal evidence for an increase of the 6.4 keV line flux. This evolution appears to be repeated for the on–phases.

The detection of only four cycles is not sufficient to establish any periodicity at high significance. The 25 ks is however a natural timescale of a black hole system with a black hole mass of a few times $10^7\,M_\odot$, as measured for NGC 3516 (e.g Onken et al 2003; Peterson et al 2004). The finding could potentially be important and, especially considering the evolution of the line emission, warrant a theoretical study. We adopt a simple model in which a flare is located above an accretion disc, corotating with it at a fixed radius. The flare illuminates an underlying region on the disc (or spot) which produces a reflection spectrum, including an Fe Kα line. The observed line flux and energy are both phase-dependent quantities and therefore, if the flare lasts for more than one orbital period, they will modulate periodically. We therefore interpret the characteristic timescale of 25 ks we measure as the orbital period. In the right panel of Fig. 25 we show a theoretical image constructed by considering a flare orbiting at $9\,r_g$ from the BH.
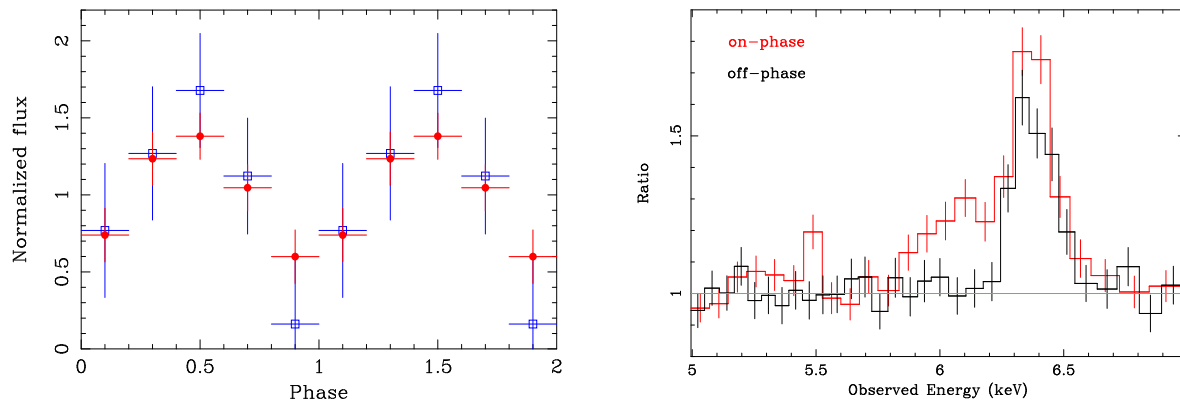
Figure 24: *Left panel*: Red feature folded light curve on 25 ks from the smoothed (red) and unsmoothed (blue) images. See Iwasawa, Miniutti & Fabian (2005) for more details. *Right panel*: The line profile (shown as a ratio to the continuum) for the on– and off–phases. The red feature is present in the on–phase only, the difference with the off–phase spectrum being above the $4\,\sigma$ level.
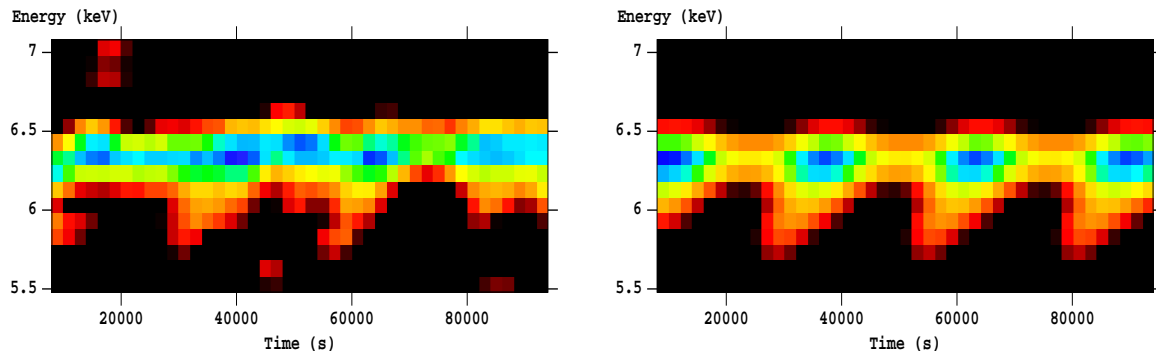

Figure 25: *Left panel*: Excess emission image in the time–energy plane from the *XMM-Newton* observation. Each pixel is 2 ks in time and 100 eV in energy. *Right panel*: Theoretical image in the time–energy plane. The theoretical model assumes the presence of a flare orbiting the BH at 9 r_g and at an height of 6 r_g plus a constant line core at 6.4 keV. The match with the observed image (left) is surprisingly good.

The theoretical model matches the data well enough. It is also possible that the emitting spot is not due to illumination from a flare but to some structure with enhanced emissivity (due to reflection of a more central continuum) on the disc itself (overdensity, spiral wave, etc).

By constructing a large number of theoretical images and comparing them with the data we could constrain the location of the reflecting spot (or illuminating flare) in the range 7–16 r_g from the BH. By combining this result with the timescale of 25 ks and by assuming this is the orbital period, the mass of the central BH in NGC 3516 can be estimated to be $1\text{--}5 \times 10^7 M_\odot$, in excellent agreement with results obtained through reverberation mapping of optical emission lines. The estimates of M_{BH} in NGC 3516 from reverberation mapping lie in the range between $1 \times 10^7\ M_\odot$ and $4 \times 10^7\ M_\odot$. Onken et al (2003) derive a value of $(1.68 \pm 0.33) \times 10^7\ M_\odot$, while Peterson et al (2004) estimate $(4.3 \pm 1.5) \times 10^7\ M_\odot$. The previous analysis based on Hβ alone gave $2.3 \times 10^7\ M_\odot$ (Ho 1999; no uncertainty is given). It is remarkable that our estimate of the black hole mass in NGC 3516 is in excellent agreement with the above results. Although the systematic flux and energy variability we report here is only tentative, the above agreement supports our interpretation.

Events like this happening at smaller radii where gravity is stronger are at present beyond the capabilities of X–ray observatories as is X–ray (Fe line) reverberation mapping (Reynolds et al 1999; Young

& Reynolds 2000). It is clear from the results presented above that the potential of future missions with much larger collecting area than XMM–Newton in the Fe K band, such as XEUS/Constellation–X, is outstanding. The prospects of probing the strong gravity regime of General Relativity via X–ray observations look stronger now than ever before.

9 Summary

A relativistically-broadened iron line is unambiguous in the spectra and behaviour of a few objects. The strength and breadth of reflection features is strong evidence for gravitational light bending and redshifts from a few r_{g}. They indicate that a dense disc extends close to the black hole, which must therefore be rapidly spinning ($a/m > 0.8$). Roy Kerr's solution to the Einstein equations in vacuum appears to be the astrophysically relevant one and the key ingredient in Galactic and extra–Galactic powerful sources of radiation.

The potential for understanding the accretion flow close to a black hole is enormous. Current observations are at the limit of *XMM-Newton* powers, which nevertheless has enabled a breakthrough in understanding the spectral behaviour of MCG–6-30-15 and similar objects. Similarities in the spectral and timing properties of AGN and BHC is enabling further progress to be made. Studies in the near future with *Suzaku* followed by XEUS/Constellation-X in the next decade will continue to open up the immediate environment of accreting black holes, within just a few gravitational radii, to detailed study.

References

[] Agol E., Krolik J.H., 2000, ApJ, 528, 161
[] Antonucci R.R., 1993, ARA&A, 31, 473
[] Balestra I., Bianchi S., Matt G., 2004, A&A, 415, 437
[] Ballantyne D.R., Ross R.R., Fabian A.C., 2001, MNRAS, 327, 10
[] Ballantyne D.R., Fabian A.C., Iwasawa K., 2004, MNRAS, 354, 839
[] Bardeen J.M., Press W.H., Teukolsky S.A., 1972, ApJ, 178, 347
[] Beckwith K., Done C., 2004, MNRAS, 352, 353
[] Beloborodov A.M., 1999, ApJ, 510, L123
[] Bianchi S., Matt G., Haardt F., Maraschi L., Nicastro F., Perola G.C., Petrucci P.O., Piro L., 2001, A&A, 376, 77
[] Bianchi S., Miniutti G., Fabian A.C., Iwasawa K., 2005, MNRAS, 360, 380
[] Blandford R.D., Znajek R.L., 1977, MNRAS, 179, 433
[] Boller Th. et al, 2002, MNRAS, 329, L1
[] Brusa M., Gilli R., Comastri A., 2005, ApJ, 621, L5
[] Carter B., 1968, Phys. Rev., 174, 1559
[] Charles P., Proc. ESO workshop on "Black Hole Binaries and AGN", 2001, Springer, 27, eds. Kaper L., van den Heuvel E.P.J., Woudt P.A.,
[] Cunningham C.T., 1975, ApJ, 202, 788
[] Cunningham C.T., 1976, ApJ, 208, 534
[] Czerny B., Nikolajuk M., Rózańska A., Dumont A.-M., 2003, A&A, 412, 317
[] Dabrowski Y., Fabian A.C., Iwasawa K., Lasenby A.N., Rynolds C.S., 1997, MNRAS, 288, L11

[] Dabrowski Y., Lasenby A.N., 2001, MNRAS, 321, 605

[] Done C., 2001, Adv. Space. Res., 28, 255

[] Dovčiak M., Bianchi S., Guainazzi M., Karas V., Matt G., 2004, MNRAS, 350, 745

[] Dovčiak M., Karas V., Yaqoob T., 2004, ApJSS, 153, 205

[] Dumont A.-M., Collin S., Paletou F., Coupé S., Godet O., Pelat D., 2003, A&A, 407, 13

[] Fabian A.C., Rees M.J., Stella L., White N.E., 1989, MNRAS, 238, 729

[] Fabian A.C., Nandra K., Reynolds C.S., Brandt W.N., Otani C., Tanaka Y., Inoue H., Iwasawa K., 1995, MNRAS, 277, L11

[] Fabian A.C., Iwasawa K., Reynolds C.S., Young A.J., 2000, PASP, 112, 1145

[] Fabian A.C., et al. 2002a, MNRAS, 335, L1

[] Fabian A.C., Ballantyne D.R., Merloni A., Vaughan S., Iwasawa K., Boller Th., 2002b, MNRAS, 331, L35

[] Fabian A.C., Vaughan S., 2003, MNRAS, 340, L28

[] Fabian A.C., Miniutti G., Gallo L., Boller Th., Tanaka Y., Vaughan S., Ross R.R., 2004, MNRAS, 353, 1071

[] Fabian A.C., Miniutti G., Iwasawa K., Ross R.R., 2005, MNRAS in press, astro-ph/0504472

[] Fender R.P., Belloni T.M., Gallo E., 2004, MNRAS, 355, 1105

[] Gallo L., Tanaka Y., Boller Th., Fabian A.C., Vaughan S., Brandt W.N., 2004, MNRAS, 353, 1064

[] Gammie C.F., 1999, ApJ, 522, L57

[] Garofalo D., Reynolds C.S., 2005, 624, 94

[] George I.M., Fabian A.C., 1991, MNRAS, 249, 352

[] Ghisellini G., Haardt F., Matt G., 2004, A&A, 413, 535

[] Gierliński M., Done C., 2004, MNRAS, 349, L7

[] Guainazzi M., 2003, A&A, 401, 903

[] Guilbert P.W., Rees M.J., 1988, MNRAS, 233, 475

[] Haardt F., Maraschi L., 1991, ApJ, 380, L51

[] Haardt F., Maraschi L., 1993, ApJ, 413, 507

[] Halpern J.P., 1984, ApJ, 281, 90

[] Ho L., 1999, in "Observational Evidence for Black Holes in the Universe", eds S. Chakrabarti, 157, Dordrecht: Reidel

[] Iwasawa K., Fabian A.C., Mushotzky R.F., Brandt W.N., Awaki K., Kunieda H., 1996a, MNRAS, 279, 837

[] Iwasawa K., et al. 1996b, MNRAS, 282, 1038

[] Iwasawa K., Fabian A.C., Young A.J., Inoue H., Matsumoto C., 1999, MNRAS, 307, 611

[] Iwasawa K., Lee J.C., Young A.J., Reynolds C.S., Fabian A.C., 2004, MNRAS, 347, 411

[] Iwasawa K., Miniutti G., 2004, Progr. Theor. Phys., S155, 247

[] Iwasawa K., Miniutti G., Fabian A.C., 2004, MNRAS, 355, 1073

[] Jiménez–Bailón E., Piconcelli E., Guainazzi M., Schartel N., Rodríguez–Pascual P.M., Santos–Lleó M., 2005, A&A, 435, 449

[] Kaastra J.S., Mewe R., Liedhal D.A., Komossa S., Brinkman A.C., 2000, A&A, 354, L83

[] Kallman T.R., Krolik J.H., 1986, NASA GSFC Lab. for High Energy Physics Spec. Rep. (*http://heasarc.gsfc.nasa.gov/docs/software/xstar/xstar.html*)

[] Kaspi S. et al, 2001, ApJ, 554, 216

[] Kerr R.P., 1963, Phys. Rev. Lett., 11, 237

[] Kinkhabwala A. et al, 2002, ApJ, 575, 732

[] Krolik J.H., 1999, ApJ, 515, L73

[] Krolik J.H., Hawley J.F., 2002, ApJ, 573, 754

[] Lamer G., McHardy I.M., Uttley P., Jahoda K., 2003, MNRAS, 338, 323

[] Laor A., 1991, ApJ, 376, 90

[] Li L., 2003, Phys. Rev., D67, 044007

[] Lightman A.P., White T.R., 1988, ApJ, 335, 57

[] Longinotti A.L., Cappi M., Nandra K., Dadina M., Pellegrini S., 2003, A&A, 410, 471

[] Longinotti A.L., Nandra K., Petrucci P.O., O'Neill P.M., 2004, MNRAS, 355, 929

[] Markoff S., Falcke H., Fender R.P., 2001, A&A, 372, L25

[] Martocchia A., Karas V., Matt G., 2000, MNRAS, 312, 817

[] Martocchia A., Matt G., Karas V., 2002, A&A, 383, L23

[] Martocchia A., Matt G., Karas V., Belloni T., Feroci M., 2002, A&A, 387, 215

[] Matsumoto C., Inoue H., Fabian A.C., Iwasawa K., 2003, PASJ, 55, 615

[] Matt G., Perola G.C., Piro L., 1991, A&A, 247, 25

[] Matt G., Perola G.C., 1992, MNRAS, 259, 433

[] Matt G., Fabian A.C., Ross R.R., 1993, MNRAS, 262, 179

[] Matt G., Fabian A.C., Ross R.R., 1996, MNRAS, 278, 1111

[] McHardy I.M., Gunn K.F., Uttley P., Goad M.R., 2005, MNRAS, 359, 1469

[] Merloni A., Fabian A.C., 2001a, MNRAS, 321, 549

[] Merloni A., Fabian A.C., 2001b, MNRAS, 328, 958

[] Merloni A., Fabian A.C., 2003, MNRAS, 342, 951

[] Miller, J.M., et al. 2002a, ApJ, 570, L69

[] Miller, J.M., et al. 2002b, ApJ, 577, L15

[] Miller, J.M., et al. 2002c, ApJ, 578, 348

[] Miller, J.M., et al. 2003, MNRAS, 338, 7

[] Miller, J.M., et al. 2004a, ApJ, 601, 450

[] Miller, J.M., et al. 2004b, ApJ, 606, L131

[] Miller J.M., Fabian A.C., Nowak M.A., Lewin W.H.G., Proc. of the 10th Marcel Grossman Meeting, 20–26 July 2003, Rio de Janeiro, Brazil, astro-ph/0402101

[] Miniutti G., Fabian A.C., Goyder R., Lasenby A.N., 2003, MNRAS, 344, L22

[] Miniutti G., Fabian A.C., 2004, MNRAS, 349, 1435

[] Miniutti G., Fabian A.C., Miller J.M., 2004, MNRAS, 351, 466

[] Miniutti G., Fabian A.C., 2005, submitted to MNRAS

[] Misner C.W., Thorne K.S., Wheeler J.A., 1973, *Gravitation*, W.H. Freeman & Co., San Francisco

[] Nandra K., George I.M., Mushotzky R.F., Turner T.J., Yaqoob T., 1997a, ApJ, 476, 70

[] Nandra K., Mushotzky R.F., Yaqoob T., George I.M., Turner T.J., 1997b, MNRAS, 284, L7

[] Nandra K., George I.M., Mushotzky R.F., Turner T.J., Yaqoob T., 1999, ApJ, 524, 707

[] Nayakshin S., Kazanas D., Kallman T.R., 2000, ApJ, 537, 833

[] Nayakshin S., Kazanas D., 2001, ApJ, 553, 885

[] Nowak M.A., 1995, PASP, 107, 1207

[] Onken C.A., Petereson B.M., Dietrich M., Robinson A., Salamanca I.M., 2003, ApJ, 585, 121

[] Orosz J.A., McClintock J.E., Remillard R.A., Corbel S., 2004, ApJ, 616, 376

[] Page D.N., Thorne K.S., 1974, ApJ, 191, 499

[] Page K.L., O'Brien P.T., Reeves J.N., Turner M.J.L., 2004, MNRAS, 347, 316

[] Peterson B.M. et al, 2004, ApJ, 613, 682

[] Petrucci P.O. et al, 2002, A&A, 338, L5

[] Ponti G., Cappi M., Dadina M., Malaguti G., 2004, A&A, 417, 451

[] Ponti G. et al, 2005, submitted to MNRAS

[] Porquet D., Reeves J.N., Uttley P., Turner T.J., 2004a, A&A, 427, 101

[] Porquet D., Reeves J.N., O'Brien P., Brinkmann W., 2004b, A&A, 422, 85

[] Pounds K.A., Reeves J.N., Page K.L., O'Brien P.T., 2004a, ApJ, 605, 670

[] Pounds K.A., Reeves J.N., King A.R., Page K.L., 2004b, MNRAS, 350, 10

[] Pringle J.E., 1981, ARA&A, 19, 137

[] Reeves J.N., Nandra K., George I.M., Pounds K.A., Turner T.J., Yaqoob T., 2004, ApJ, 602, 648

[] Reynolds C.S., 1996, PhD thesis, University of Cambridge

[] Reynolds C.S., 1997, MNRAS, 286, 513
[] Reynolds C.S., Begelman M.C., 1997, ApJ, 488, 109
[] Reynolds C.S., Young A.J., Begelman M.C., Fabian A.C., 1999, ApJ, 514, 164
[] Reynolds C.S., 2000, ApJ, 533, 811
[] Reynolds C.S., Nowak M.A., 2003, Phys. Rep., 377, 389
[] Reynolds C.S., Wilms J., Begelman M.C., Staubert R., Kendziorra E., 2004, MNRAS, 349, 1153
[] Ross R.R., Fabian A.C., 1993, MNRAS, 261, 74
[] Ross R.R., Fabian A.C., Young A.J., 1999, MNRAS, 306, 461
[] Ross R.R., Fabian A.C., 2005, MNRAS, 358, 211
[] Rossi S., Homan J., Miller J.M., Belloni T., 2005, MNRAS in press, astro-ph/0504182
[] Rózańska A., Dumont A.-M., Czerny B., Bollin S., 2002, MNRAS, 332, 799
[] Ruszkowski M., 2000, MNRAS, 315, 1
[] Schwarzschild K., 1916, Kl. Math, Phys. Tech., 189
[] Shakura N.I., Sunyaev R., 1973, A&A, 24, 337
[] Shemmer O., Netzer H., Maiolino R., Oliva E., Croom S., Corbett E., di Fabrizio L., 2004, ApJ, 614, 547
[] Shih D.C., Iwasawa K., Fabian A.C., 2001, MNRAS, 333, 687
[] Stella L., 1990, Nature, 344, 747
[] Streblyanska A., Hasinger G., Finoguenov A., Barcons X., Mateos S., Fabian A.C., 2005, A&A, 432, 395
[] Tanaka Y., et al. 1995, Nature, 375, 659
[] Tanaka Y., Gallo L., Boller Th., Keil R., Ueda Y., 2004, PASJ, 56, L9
[] Taylor R.D., Uttley P., McHardy I.M., 2003, MNRAS, 342, L31
[] Thorne K.S., 1974, ApJ, 191, 507
[] Turner A.K., Fabian A.C., Vaughan S., Lee J.C., 2003, MNRAS, 346, 833
[] Turner A.K., Fabian A.C., Lee J.C., Vaughan S., 2004, MNRAS, 353, 319
[] Turner T.J. et al, 2002, ApJ, 574, L123
[] Turner T.J., Kraemer S.B., Reeves J.N., 2004, ApJ, 603, 62
[] Turner T.J., Kraemer S.B., George I.M, Reeves J.N., Bottorff M.C., 2005, ApJ, 618, 155
[] Uttley P., McHardy I.M., 2004, Progr. Th. Phys. S155, 170
[] Vaughan S., Edelson R., 2001, ApJ, 548, 694
[] Vaughan S., Fabian A.C., Nandra K., 2003, MNRAS, 339, 1237
[] Vaughan S., Fabian A.C., 2004, MNRAS, 348, 1415
[] Vaughan S., Fabian A.C., Ballantyne D.R., de Rosa A., Piro L., Matt G., 2004, MNRAS, 351, 193
[] Volonteri M., Madau P., Quataert E., Rees M.J., 2005, ApJ, 620, 69
[] Walter R., Fink H.H., 1993, A&A, 274, 105
[] Wilms J., et al. 2001, MNRAS, 328, L27
[] Yaqoob T., George I.M., Kallman T.R., Padmanabhan U., Weaver K.A., Turner T.J., 2003, ApJ, 596, 85
[] Yaqoob T., Padmanabhan U., 2004, ApJ, 604, 63
[] Young A.J., Ross R.R., Fabian A.C., 1998, MNRAS, 300, L11
[] Young A.J., Reynolds C.S., 2000, ApJ, 529, 101
[] Young A.J., Lee J.C., Fabian A.C., Reynolds C.S., Gibson R.R., Canizares C.R., 2005, ApJ in press, astro-ph/0506082
[] Zdziarski A.A. et al, 1994, MNRAS, 269, L55
[] Zycki P.T., Krolik J.H., Zdziarski A.A., Kallman T.R., 1994, ApJ, 437, 597